YEAST MEIOSIS

Sister kinetochores are mechanically fused during meiosis I in yeast

Krishna K. Sarangapani,[1]* Eris Duro,[2]* Yi Deng,[1] Flavia de Lima Alves,[2] Qiaozhen Ye,[3] Kwaku N. Opoku,[1] Steven Ceto,[4]† Juri Rappsilber,[2,5] Kevin D. Corbett,[3,6] Sue Biggins,[4,7] Adèle L. Marston,[2]‡ Charles L. Asbury[1]‡

Production of healthy gametes requires a reductional meiosis I division in which replicated sister chromatids comigrate, rather than separate as in mitosis or meiosis II. Fusion of sister kinetochores during meiosis I may underlie sister chromatid comigration in diverse organisms, but direct evidence for such fusion has been lacking. We used laser trapping and quantitative fluorescence microscopy to study native kinetochore particles isolated from yeast. Meiosis I kinetochores formed stronger attachments and carried more microtubule-binding elements than kinetochores isolated from cells in mitosis or meiosis II. The meiosis I–specific monopolin complex was both necessary and sufficient to drive these modifications. Thus, kinetochore fusion directs sister chromatid comigration, a conserved feature of meiosis that is fundamental to Mendelian inheritance.

The hallmark of meiosis is a twofold reduction in ploidy, which occurs because one round of DNA replication is followed by two rounds of chromosome segregation. Sister chromatids distinctly comigrate during meiosis I, thereby enabling segregation of homologous chromosomes. During meiosis II, which resembles mitosis, the sister chromatids separate (fig. S1, A and B). It has been suggested that the comigration of sister chromatids during meiosis I depends on fusion of sister kinetochores in a range of organisms (*1*–*4*) (fig. S1C). Because fused sister kinetochore pairs would contain more microtubule-binding elements than individual kinetochores, we reasoned that they might form stronger attachments to microtubules. Alternatively, if one kinetochore within each sister pair was selectively inactivated during meiosis I (*5*, *6*), then the remaining active kinetochores would probably form attachments with similar strength relative to individual mitotic and meiosis II kinetochores.

To distinguish between the "fusion" and "one-sister shut-off" mechanisms, we purified native kinetochore particles from yeast cells arrested in metaphase of meiosis I (via meiosis-specific depletion of Cdc20) (*7*), using methods developed for the isolation of mitotic particles (*8*, *9*). The purified material contained essentially all known kinetochore components (table S1), and its bulk composition was very similar to material isolated from mitosis (Fig. 1A; fig. S2, A and B; and table S1). We used fluorescence- and laser trap–based assays to determine whether the meiosis I kinetochore particles remained functional in vitro. As shown previously for mitotic particles (*8*), fluorescently labeled particles isolated from meiosis I cultures bound specifically to microtubules and tracked processively with disassembling microtubule tips (Fig. 1B and movie S1). Furthermore, meiosis I kinetochore particles formed load-bearing attachments to microtubule tips, supporting forces up to 15 pN and persisting through "catastrophe" and "rescue" events, in which the filament switched from assembly to disassembly and vice versa (Fig. 1C). Thus, native kinetochore particles isolated from meiotic cultures are functional. The meiotic particles formed very-long-lived tip attachments with a mean lifetime of 52 ± 23 min at 7 pN of tension, double the lifetime measured previously for mitotic particles (26 ± 6 min) at a similar level of tension (7.2 pN) (*8*).

The long lifetimes of attachments formed by meiosis I kinetochore particles suggested that they may be stronger than particles from mitotic cells. To assess their strength directly, we attached the meiosis I kinetochore particles to growing microtubule tips and tested them using a force ramp, where force was increased at a constant rate until the attachments ruptured (Fig. 1D). Control kinetochore particles isolated from metaphase-arrested mitotic cells ruptured at an average force of 9.4 ± 0.4 pN (Fig. 2B), which is indistinguishable from the strength of particles harvested during vegetative (asynchronous mitotic) growth (*8*). Rupture strengths were unaffected by differences in ploidy and were relatively insensitive to the method of mitotic cell cycle arrest (fig. S3). Meiosis I particles, however, formed significantly stronger attachments, rupturing at forces ranging from 6.5 to 22 pN (i.e., up to the load limit of our laser trap), with an average of 13.1 ± 0.3 pN (Fig. 2, A and B, and table S2). Mean rupture forces for both meiosis I and mitotic particles remained invariant as the density of particles on the beads was reduced below the single-particle limit (fig. S4), indicating that higher strength is an intrinsic property of individual meiosis I kinetochore particles.

To determine whether the higher kinetochore attachment strength is specific to meiosis I or persists into meiosis II, we prepared synchronized meiotic cultures by releasing cells from a prophase I block (*10*, *11*). Particles harvested from synchronized metaphase I cells formed attachments that ruptured at 13.1 ± 0.6 pN, on average (Fig. 2, A and B, meiosis I*). However, particles from synchronized metaphase II cells ruptured at 9.3 ± 0.7 pN, on average (Fig. 2, A and B, meiosis II*). Thus, the higher intrinsic strength of kinetochore particles occurs specifically during meiosis I and returns to mitotic-like levels as cells progress into meiosis II.

If the particles isolated from meiosis I cells are fused sister kinetochore pairs, they should contain more microtubule binding elements than mitotic particles. We purified fluorescent particles doubly tagged with SNAP-549 on Nuf2 (a subunit of the microtubule-binding Ndc80 complex) and CLIP-647 on Mif2 (an inner kinetochore component orthologous to CENP-C). Spore viability was unaffected, and rupture strengths for the fluorescent particles were indistinguishable from untagged particles (fig. S5 and table S2), indicating no loss of functionality. The purified kinetochore material contained a mixture of dual-color particles carrying both Nuf2 and Mif2, plus subcomplexes lacking Nuf2 or Mif2 (Fig. 2C). Subcomplexes with just one detectable Nuf2 [identifiable by their single-step photobleaching behavior (fig. S6)] served as internal controls, allowing normalization of particle brightnesses into estimates for the approximate numbers of Nuf2 molecules associated with each particle. Dual-color particles from meiosis I cells carried more Nuf2 molecules, on average [6.5 ± 2.8 (mean ± SD from N = 4 preparations)], than those from vegetatively growing cells, which had 3.8 ± 1.3 (N = 4) (Fig. 2, D and E). The apparent Nuf2 content was variable and lower than in vivo estimates [which suggest 8 to 20 copies per mitotic kinetochore (*12*, *13*)]. However, consistent with the fusion model, Nuf2 content was significantly higher for dual-color meiosis I particles than for vegetative particles prepared in tandem, by a factor of 1.66 ± 0.26 (mean ± SD, N = 4 tandem pairs; P = 0.014 by t test).

If fusion of sister kinetochore pairs underlies the increased strength of meiosis I kinetochore particles, the increase should vanish if the particles are harvested from cells in which every kinetochore lacks a sister. We engineered cells to undergo meiosis without replicating their DNA [via meiosis-specific depletion of Cdc6 (*14*), part of the prereplicative complex (*15*)]. Because the lack of sister chromatids precludes homology-based DNA repair (*16*), we also deleted the Spo11 endonuclease, thereby avoiding high levels of DNA damage that might interfere with meiotic progression. Spo11 catalyzes formation of the chiasmata that link homologous chromosomes

[1]Department of Physiology and Biophysics, University of Washington, Seattle, WA 98195, USA. [2]Wellcome Trust Centre for Cell Biology, University of Edinburgh, Edinburgh, UK. [3]Ludwig Institute for Cancer Research, San Diego Branch, La Jolla, CA 92093, USA. [4]Division of Basic Sciences, Fred Hutchinson Cancer Research Center, Seattle, WA 98109, USA. [5]Institute of Bioanalytics, Department of Biotechnology, Technische Universität Berlin, Berlin, Germany. [6]Department of Cellular and Molecular Medicine, University of California, San Diego, La Jolla, CA 92093, USA. [7]Department of Biochemistry, University of Washington, Seattle, WA 98195, USA.
*These authors contributed equally to this work. †Present address: Department of Neurosciences, University of California, San Diego, CA 92093, USA. ‡Corresponding author. E-mail: casbury@u.washington.edu (C.L.A.); adele.marston@ed.ac.uk (A.L.M.)

(*17*), so its deletion (*spo11*Δ) enabled us to test whether tension across homologs is required for sister kinetochore fusion (*18*). Kinetochore particles from *spo11*Δ cells were identical in strength to those from wild-type cells, indicating that linkage between homologs (and, thus, spindle-generated tension across them) was dispensable for the high attachment strength of meiosis I kinetochores (Fig. 2, A and B, *no chiasmata*).

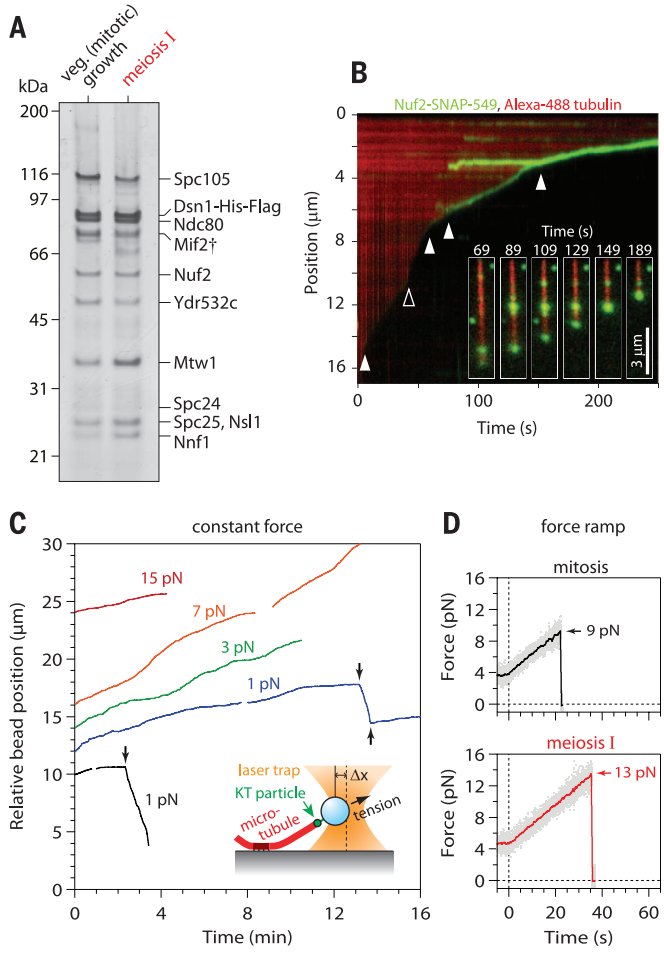

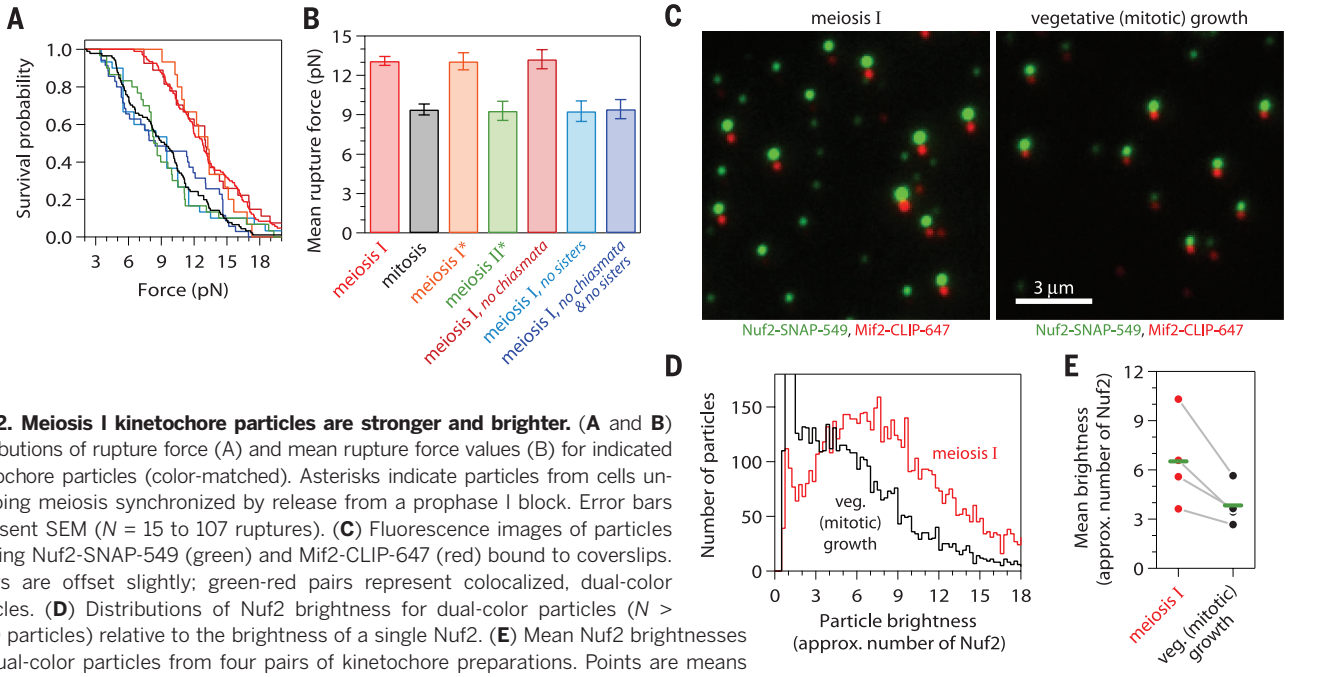

Fig. 1. Native kinetochore particles from meiotic cells recapitulate tip-coupling in vitro. (**A**) Core kinetochore proteins copurified from cells undergoing vegetative (mitotic) growth and cells arrested in metaphase I of meiosis, visualized by silver-stained SDS–polyacrylamide gel electrophoresis (*9*). Mif2 (†) comigrates with nonspecific background proteins (*8*). kDa, kilodaltons. (**B**) Kymograph showing movement of fluorescent meiosis I kinetochore particles (green) driven by a disassembling microtubule (red) (see movie S1). Filled arrowheads mark tip-particle encounters; the open arrowhead denotes particle release. Insets shows images at indicated times. (**C**) Position versus time for tip-attached meiosis I particles tested with a force clamp at indicated loads. Arrows mark catastrophes and rescue. Intervals when the laser trap was briefly shuttered (to clear debris) appear as gaps in the 1- and 7-pN traces. The inset shows a schematic of the assay (*9*). KT, kinetochore. (**D**) Tensile force versus time for indicated particles bound to assembling tips and tested with a 0.25–pN s^{-1} force ramp. Gray dots show raw data; colored traces show the same data after smoothing (500-ms sliding boxcar average). Dashed vertical lines mark the start of the force ramp. Arrows denote rupture.

Fig. 2. Meiosis I kinetochore particles are stronger and brighter. (**A** and **B**) Distributions of rupture force (A) and mean rupture force values (B) for indicated kinetochore particles (color-matched). Asterisks indicate particles from cells undergoing meiosis synchronized by release from a prophase I block. Error bars represent SEM (N = 15 to 107 ruptures). (**C**) Fluorescence images of particles carrying Nuf2-SNAP-549 (green) and Mif2-CLIP-647 (red) bound to coverslips. Colors are offset slightly; green-red pairs represent colocalized, dual-color particles. (**D**) Distributions of Nuf2 brightness for dual-color particles (N > 4900 particles) relative to the brightness of a single Nuf2. (**E**) Mean Nuf2 brightnesses for dual-color particles from four pairs of kinetochore preparations. Points are means from individual preparations. Gray lines connect means from particles prepared in tandem (*9*); green horizontal lines are means across all preparations.

However, high strength was lost when meiosis I particles were harvested from *cdc6-meiotic-null* cells (Fig. 2, A and B, *no sisters* or *no chiasmata & no sisters*). Thus, sister kinetochores are required for the increased strength of meiosis I kinetochore particles, as predicted by the fusion model.

The meiosis I–specific monopolin complex consists of four proteins (Mam1, Csm1, Lrs4, and Hrr25) (*5*, *19*–*21*) with twin kinetochore-binding sites that have been proposed to directly cross-link sister kinetochores in budding yeast (*1*, *5*, *20*, *22*). However, because the receptor for monopolin, Dsn1 (*1*, *23*), is present in multiple copies in the kinetochore (*12*), another possibility is that the twin monopolin sites bind to the same kinetochore and inactivate it, thereby shutting off one of the two sister kinetochores (fig. S1C) (*5*, *6*).

Monopolin was detectable at low levels in kinetochore material from meiosis I cultures (fig. S2C). To test the impact of monopolin on the behavior of kinetochore particles, we genetically disrupted its function in three ways (*mam1*Δ, *csm1-L161D*, and *dsn1-*Δ*N*), all of which disrupt sister comigration during meiosis I (*1*, *21*, *23*). In all cases, we found that the high 13-pN strength of meiosis I kinetochore particles was lost and their strength returned to mitosis-like levels (~9 pN) (Fig. 3), confirming that monopolin is required for high attachment strength. We also engineered cells to ectopically express monopolin during mitosis by inducing expression of *MAM1* together with *CDC5* (encoding Polo kinase), which caused erroneous co-orientation in 28% of cells (*5*). Kinetochore particles isolated from these cells gave a bimodal rupture force distribution (Fig. 3A) with an intermediate average strength of 11.2 ± 0.4 pN (Fig. 3B). This observation may be explained by the incomplete penetrance of monopolin induction in these cells (*5*).

To test whether kinetochores can be fused by monopolin in the absence of other cellular factors, we recombinantly expressed and purified the four-protein monopolin complex [containing a kinase-dead Lys^{38}→Arg^{38} mutant of Hrr25 (fig. S2D)] (*22*) and incubated it with isolated kinetochore particles. Incubation with recombinant monopolin was sufficient to strengthen mitotic particles and also particles from meiosis I cells in which monopolin was disrupted (*mam1*Δ or *csm1-L161D*), raising their mean rupture forces from ~9 to ~13 pN (Fig. 4, A and B) in a dose-dependent manner (Fig. 4C). However, the same treatment did not affect the strength of particles from cells lacking the monopolin binding site on Dsn1 (*dsn1-*Δ*N*) (Fig. 4, A and B). Likewise, monopolin addition did not strengthen particles (*mam1*Δ) prelinked to laser trapping beads (Fig. 4C), presumably because immobilization on beads prevented cross-linking of the particles. When fluorescent particles from vegetatively growing cells were incubated with increasing amounts of monopolin, their average brightness grew monotonically, and the approximate number of Nuf2 molecules associated with each particle increased twofold, from 4.8 ± 0.4 to 10.9 ± 1.5 (mean ± SD, $N \geq 2$ experiments) (Fig. 4D). Thus, monopolin alone is sufficient for fusion of kinetochore particles in vitro.

Sister chromatid comigration is a universal feature of meiosis I that governs Mendelian inheritance, and its failure is a major cause of birth defects and infertility (*24*). Here we have shown

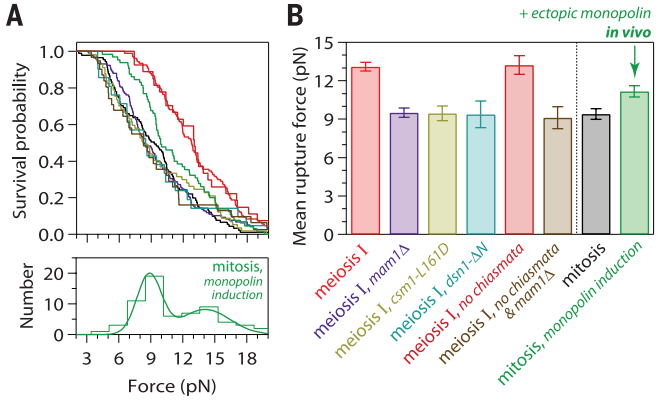

Fig. 3. Monopolin is necessary for the high strength of meiosis I kinetochore particles and is sufficient in vivo. (**A** and **B**) Distributions of rupture force (A) and mean rupture force values (B) for indicated kinetochore particles (color-matched). Data for particles from meiosis I (red), meiosis I without chiasmata (dark red), and mitosis (black) are replotted from Fig. 2, A and B, for comparison. Error bars represent SEM (N = 21 to 118 ruptures).

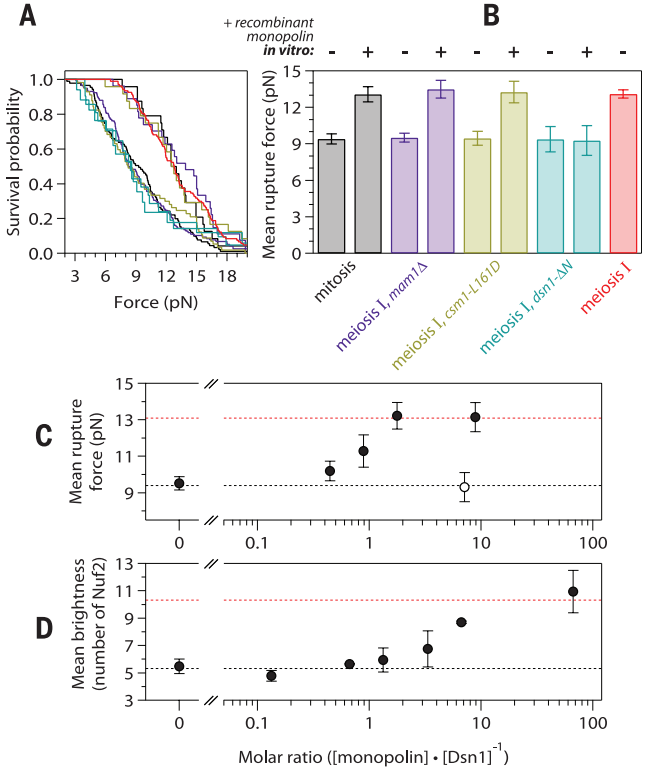

Fig. 4. Pure recombinant monopolin is sufficient to increase the strength and brightness of kinetochore particles in vitro. (**A** and **B**) Distributions of rupture force (A) and mean rupture force values (B) for kinetochore particles (color-matched) after incubation with recombinant monopolin [at molar ratio 1.8 versus Dsn1-His-Flag; "+" in (B)]. Data for particles without monopolin incubation ["-" in (B)] are replotted from Fig. 3, A and B, for comparison. Error bars represent SEM (N = 17 to 118 ruptures). (**C**) Mean rupture forces for meiosis I, *mam1*Δ kinetochore particles after incubation with indicated amounts of recombinant monopolin (*9*). Filled circles are data from particles preincubated with monopolin before linking to polystyrene laser trapping beads. The open circle shows control in which particles were first linked to trapping beads and subsequently incubated with monopolin. Error bars represent SEM (N = 28 to 118 ruptures). Dashed lines denote means for mitosis (black) and meiosis I (red) particles (from Fig. 2B). (**D**) Mean Nuf2 brightnesses for dual-color particles isolated from cells undergoing vegetative (mitotic) growth, incubated with indicated amounts of recombinant monopolin. Error bars represent SD (N = 2 or 3 experiments). Dashed lines represent mean brightnesses for dual-color vegetative (black) and meiosis I (red) kinetochore particles prepared on the same day, without monopolin incubation (from Fig. 2E).

that a meiosis I–specific factor from budding yeast, monopolin, generates kinetochores with more microtubule-binding elements and greater strength. These findings provide direct evidence that sister kinetochore fusion underlies the cosegregation of sister chromatids during meiosis I.

REFERENCES AND NOTES

1. K. D. Corbett *et al*., *Cell* **142**, 556–567 (2010).
2. X. Li, R. K. Dawe, *Nat. Cell Biol.* **11**, 1103–1108 (2009).
3. L. S. Goldstein, *Cell* **25**, 591–602 (1981).
4. L. V. Paliulis, R. B. Nicklas, *J. Cell Biol.* **150**, 1223–1232 (2000).
5. F. Monje-Casas, V. R. Prabhu, B. H. Lee, M. Boselli, A. Amon, *Cell* **128**, 477–490 (2007).
6. M. Winey, G. P. Morgan, P. D. Straight, T. H. Giddings Jr., D. N. Mastronarde, *Mol. Biol. Cell* **16**, 1178–1188 (2005).
7. B. H. Lee, A. Amon, *Science* **300**, 482–486 (2003).
8. B. Akiyoshi *et al*., *Nature* **468**, 576–579 (2010).
9. Materials and methods are available as supplementary materials on *Science* Online.
10. T. M. Carlile, A. Amon, *Cell* **133**, 280–291 (2008).
11. K. R. Benjamin, C. Zhang, K. M. Shokat, I. Herskowitz, *Genes Dev.* **17**, 1524–1539 (2003).
12. A. P. Joglekar, D. C. Bouck, J. N. Molk, K. S. Bloom, E. D. Salmon, *Nat. Cell Biol.* **8**, 581–585 (2006).
13. J. Lawrimore, K. S. Bloom, E. D. Salmon, *J. Cell Biol.* **195**, 573–582 (2011).
14. A. Hochwagen, W. H. Tham, G. A. Brar, A. Amon, *Cell* **122**, 861–873 (2005).
15. J. H. Cocker, S. Piatti, C. Santocanale, K. Nasmyth, J. F. Diffley, *Nature* **379**, 180–182 (1996).
16. T. Goldfarb, M. Lichten, *PLOS Biol.* **8**, e1000520 (2010).
17. S. Keeney, C. N. Giroux, N. Kleckner, *Cell* **88**, 375–384 (1997).
18. M. A. Shonn, R. McCarroll, A. W. Murray, *Science* **289**, 300–303 (2000).
19. M. Petronczki *et al*., *Cell* **126**, 1049–1064 (2006).
20. K. P. Rabitsch *et al*., *Dev. Cell* **4**, 535–548 (2003).
21. A. Tóth *et al*., *Cell* **103**, 1155–1168 (2000).
22. K. D. Corbett, S. C. Harrison, *Cell Reports* **1**, 583–589 (2012).
23. S. Sarkar *et al*., *PLOS Genet.* **9**, e1003610 (2013).
24. K. T. Jones, S. I. Lane, *Development* **140**, 3719–3730 (2013).

ACKNOWLEDGMENTS

We thank A. Hoskins, M. Miller, N. Umbreit, and E. Yusko for helpful comments. We thank A. Desai for providing antibodies and A. Hoskins for SNAPf and CLIPf plasmids. The Wellcome Trust supported this work through a Sir Henry Wellcome Fellowship to E.D. (096078), Senior Research Fellowships to A.L.M. (090903) and J.R. (084229), and two Wellcome Trust Centre Core Grants (077707 and 092076) and an instrument grant (091020). The work was also supported by NIH grants to C.L.A. (R01GM079373 and S10RR026406), S.B. (R01GM064386), and K.D.C. (R01GM104141) and by a Packard Fellowship to C.L.A. (2006-30521). K.D.C. also acknowledges support from the Ludwig Institute for Cancer Research and the Sidney Kimmel Foundation. Additional data described in this work can be found in the supplementary materials. E.D., K.K.S., S.B., A.L.M., and C.L.A. conceived the experiments. E.D. generated new yeast strains and isolated kinetochore particles. K.K.S. performed laser trap experiments. Y.D. performed the fluorescence measurements. F.d.L.A. and J.R. performed proteomics analysis. Q.Y. and K.D.C. purified monopolin. K.N.O. and S.C. optimized fluorescent labeling of kinetochore particles. E.D., K.K.S., A.L.M., and C.L.A. prepared the manuscript.

SUPPLEMENTARY MATERIALS

www.sciencemag.org/content/346/6206/248/suppl/DC1
Materials and Methods
Figs. S1 to S8
Tables S1 to S3
References (*25*–*42*)
Movie S1
Additional Data Tables S1 to S3

30 May 2014; accepted 1 September 2014
Published online 11 September 2014;
10.1126/science.1256729

LUNG CANCER EVOLUTION

Spatial and temporal diversity in genomic instability processes defines lung cancer evolution

Elza C. de Bruin,[1]* Nicholas McGranahan,[2,3]* Richard Mitter,[2]* Max Salm,[2]* David C. Wedge,[4]* Lucy Yates,[4,5]† Mariam Jamal-Hanjani,[1]† Seema Shafi,[1] Nirupa Murugaesu,[1] Andrew J. Rowan,[2] Eva Grönroos,[2] Madiha A. Muhammad,[1] Stuart Horswell,[2] Marco Gerlinger,[2] Ignacio Varela,[6] David Jones,[4] John Marshall,[4] Thierry Voet,[4,7] Peter Van Loo,[4,7] Doris M. Rassl,[8] Robert C. Rintoul,[8] Sam M. Janes,[9] Siow-Ming Lee,[1,10] Martin Forster,[1,10] Tanya Ahmad,[10] David Lawrence,[10] Mary Falzon,[10] Arrigo Capitanio,[10] Timothy T. Harkins,[11] Clarence C. Lee,[11] Warren Tom,[11] Enock Teefe,[11] Shann-Ching Chen,[11] Sharmin Begum,[2] Adam Rabinowitz,[2] Benjamin Phillimore,[2] Bradley Spencer-Dene,[2] Gordon Stamp,[2] Zoltan Szallasi,[12,13] Nik Matthews,[2] Aengus Stewart,[2] Peter Campbell,[4] Charles Swanton[1,2]‡

Spatial and temporal dissection of the genomic changes occurring during the evolution of human non–small cell lung cancer (NSCLC) may help elucidate the basis for its dismal prognosis. We sequenced 25 spatially distinct regions from seven operable NSCLCs and found evidence of branched evolution, with driver mutations arising before and after subclonal diversification. There was pronounced intratumor heterogeneity in copy number alterations, translocations, and mutations associated with APOBEC cytidine deaminase activity. Despite maintained carcinogen exposure, tumors from smokers showed a relative decrease in smoking-related mutations over time, accompanied by an increase in APOBEC-associated mutations. In tumors from former smokers, genome-doubling occurred within a smoking-signature context before subclonal diversification, which suggested that a long period of tumor latency had preceded clinical detection. The regionally separated driver mutations, coupled with the relentless and heterogeneous nature of the genome instability processes, are likely to confound treatment success in NSCLC.

Lung cancer is the leading cause of cancer-related mortality (*1*, *2*). Understanding the pathogenesis and evolution of lung cancer may lead to greater insight into tumor initiation and maintenance and may guide therapeutic interventions. Previous work characterizing the genome of non–small cell lung cancer (NSCLC) has demonstrated that NSCLC genomes exhibit hundreds of nonsilent mutations together with copy number aberrations and genome doublings (*3*–*9*). Although subclonal populations have been identified within single biopsies (*9*), the extent of genomic diversity within primary NSCLCs remains unclear. Moreover, although both exogenous mutational processes, such as smoking (*10*–*12*), and endogenous processes, such as up-regulation of APOBEC cytidine deaminases (*13*–*15*), have been found to contribute to the large mutational burden in NSCLC, the temporal dynamics of these processes and their contribution to driver somatic aberrations over time remain unknown.

To investigate lung cancer evolution, we performed multiregion whole-exome and/or whole-genome sequencing (M-seq WES/WGS) on a total of 25 tumor regions, collected from seven NSCLC patients who underwent surgical resection before receiving adjuvant therapy. The major NSCLC histological subtypes, including adenocarcinoma (LUAD) and squamous cell carcinoma (LUSC), were represented (table S1). Sequencing of tumor and normal DNA to mean coverage depths of 107× and 54× for M-seq WES and M-seq WGS, respectively (table S2), identified 1884 nonsilent and 76,129 silent mutations (*16*).

To evaluate the intratumor heterogeneity of nonsilent mutations, we classified each mutation as ubiquitous (present in all tumor regions) or heterogeneous (present in at least one, but not all, regions). Spatial intratumor heterogeneity was identified in all seven NSCLCs, with a median of 30% heterogeneous mutations (range 4

[1]Cancer Research UK Lung Cancer Centre of Excellence, University College London Cancer Institute, London WC1E 6BT, UK. [2]Cancer Research UK London Research Institute, London WC2A 3LY, UK. [3]Centre for Mathematics and Physics in the Life Science and Experimental Biology (CoMPLEX), University College London, London WC1E 6BT, UK. [4]Wellcome Trust Sanger Institute, Hinxton, CB10 1SA, UK. [5]University of Cambridge, Cambridge CB2 1TN, UK. [6]Instituto de Biomedicina y Biotecnología de Cantabria (CSIC-UC-Sodercan), Departamento de Biología Molecular, Universidad de Cantabria, Santander, Spain. [7]Department of Human Genetics, University of Leuven, 3000 Leuven, Belgium. [8]Papworth Hospital NHS Foundation Trust, Cambridge CB23 3RE, UK. [9]Lungs for Living Research Centre, University College London, London WC1E 6BT, UK. [10]University College London Hospitals, London NW1 2BU, UK. [11]Thermo Fisher Scientific, Carlsbad, CA 92008, USA. [12]Technical University of Denmark, 2800 Kongens Lyngby, Denmark. [13]Children's Hospital Informatics Program, Harvard Medical School, Boston, MA 02115, USA.
*These authors contributed equally to this work. †These authors contributed equally to this work. ‡**Corresponding author. E-mail: charles.swanton@cancer.org.uk**

Supplementary Materials for

Sister Kinetochores are Mechanically Fused During Meiosis I in Yeast

Krishna K. Sarangapani, Eris Duro, Yi Deng, Flavia de Lima Alves, Qiaozhen Ye, Kwaku N. Opoku, Steven Ceto, Juri Rappsilber, Kevin D. Corbett, Sue Biggins, Adèle L. Marston*, Charles L. Asbury*

*Corresponding author. E-mail: adele.marston@ed.ac.uk; casbury@u.washington.edu

This PDF file includes:

Other Supplementary Materials for this manuscript include the following:

Materials and Methods

Genetic methods and strains

Standard genetic techniques were used. All newly created yeast strains were isogenic with SK1; genotypes are described in Table S3. Deletions, promoter replacements and epitope tags were made using a PCR-based integration system and confirmed by PCR (*25, 26*). The 6His–3Flag epitope tagging of the endogenous *DSN1* gene was performed using PCR-based integration, as previously described (*8*), and did not affect spore viability or the co-orientation of sister centromeres during meiotic metaphase I (as judged by microscopy of GFP-tagged *CENV* foci in tetranucleate cells). Truncation of endogenous Dsn1 and its simultaneous tagging with 6His–3Flag were also performed using PCR-based integration. A *pGAL-CDC5* fusion tagged with 3MYC epitopes was integrated at the *URA3* locus (*27*). *MAM1-9MYC* (*21*), *NDC10-6HA* (*21*), the Dsn1 N-terminal truncation allele (*dsn1-ΔN*) (*23*), and the *csm1-L161D* allele (*1*), have all been previously described (*1, 21, 23*). The *ipl1-321* allele (*28*) was PCR-amplified from a W303 strain and introduced into SK1 using lithium acetate transformation (*26*). Strains with SNAPf- and CLIPf-tagged proteins were prepared as previously described (*29*).

Growth conditions

To obtain meiotic cultures, yeast strains were grown at 30°C for 16 h on YPG plates (1% yeast extract, 2% bactopeptone, 2.5% glycerol, and 2% agar) and then for 24 h on YPD4% plates (1% yeast extract, 2% bactopeptone, 4% glucose, and 2% agar). Cells were then cultured in YPD (1% yeast extract, 2% bactopeptone, and 2% glucose) for 24 h and then inoculated at an OD_{600} of 0.2–0.3 in YPA (1% yeast extract, 2% bactopeptone, and 1% potassium acetate) and grown overnight to an OD_{600} of ≥ 1.8. Cells were then harvested and re-suspended into sporulation medium (0.3% potassium acetate, pH 7) to an OD_{600} of 1.8–1.9 and induced to sporulate at 30°C. For metaphase I arrest, a meiotic shut-off allele of *CDC20* was used (*pCLB2-CDC20*; here referred to as *cdc20-meiotic-null*, or abbreviated *cdc20-mn*) (*7*). For synchronous meiosis, a pachytene block-release protocol was used: expression of the *NDT80* gene, which is required for exit from pachytene, was induced by the addition of 1 μM estradiol 6 h after inoculation of cells into sporulation medium as previously described (*10*). Mitotic cultures were prepared using either benomyl (as described (*30*)) or depletion of Cdc20. For depletion of Cdc20 in mitosis, the endogenous *CDC20* gene was tagged with an AID-degron (auxin-induced degradation) (*31*). Cells were grown overnight in liquid YPD medium to saturation, then diluted 1:200 in YP+lactate (for G1 arrest). After 16h growth, cultures were harvested and resuspended in YPD media containing 1 mM of the synthetic auxin, NAA (1-Naphthaleneacetic acid; Sigma N0640), to deplete Cdc20 and thus cause a metaphase arrest. NAA was added every hour to maintain metaphase arrest. For temperature-sensitive mutants, cultures were shifted to 37°C for 3h.

Mitotic induction of monopolin

Monopolin expression in mitosis was induced essentially as described (*5*) with minor modifications. Diploid yeast cells carrying the *CDC20-AID* and *pGAL-CDC5 pGAL-MAM1* fusions and *CENV-GFP* dots were cultured in YPDA media to saturation. Cells were then diluted 1:200 in YP+lactate (for G1 arrest); after 16h, cells were harvested and resuspended in media containing 2% galactose (to induce Cdc5 and Mam1 expression) and NAA (to deplete Cdc20, and thus cause a metaphase arrest). NAA was added every hour to maintain metaphase arrest. When metaphase arrest was complete, cells were harvested. GFP dot separation (to estimate the percentage of co-oriented and bi-oriented sister kinetochores) was also scored.

Isolation of kinetochore particles

Kinetochore particles were isolated by affinity-purifying Dsn1–6His–3Flag protein, as previously described (*8*), with minor modifications. Briefly, extract was prepared by breaking yeast cells with a Retsch ball mill (using a single 25 mm ball for 3x 3min at 30 Hz for mitotic cells or 5x 3min at 30 Hz for meiotic cells, with 10 min in liquid nitrogen in between) followed by ultracentrifugation (24,000 rpm for 90 minutes at 4°C). Beads conjugated with anti-Flag antibodies were incubated with extract for 3h with constant rotation, followed by three washes with buffer H (BH)/0.15 (25 mM HEPES, 2 mM $MgCl_2$, 0.1 mM EDTA, 0.5 mM EGTA pH 8.0, 0.1% NP-40, 150 mM KCl, 15% glycerol) containing protease inhibitors (at 10 μg mL^{-1} final concentration for each of chymostatin, leupeptin, antipain, pepstatin A, E-64, aprotinin; 2 mM final AEBSF–Pefablock, 1 mM NEM) phosphatase inhibitors (0.4 mM Na orthovanadate, 0.5 μM microcystin, 4 mM β-glycerophosphate, 2 mM Na pyrophosphate,10 mM NaF) and 2 mM dithiothreitol (DTT). Beads were further washed twice with BH/0.15 with protease inhibitors. Associated proteins were eluted from the beads by gentle agitation of beads in elution buffer (0.5 mg mL^{-1} 3Flag peptide in BH/0.15 with protease inhibitors) for 25 min at room temperature. A typical concentration of Dsn1–6His–3Flag was 2 μg mL^{-1} as determined by comparing the purified material with BSA standards on silver-stained SDS–PAGE gels.

For some of the kinetochore samples analyzed by mass spectrometry (Table S1), cross-linking with dithiobis[succinimidyl propionate] (DSP) was performed during particle preparation. Yeast cells were harvested and resuspended in 100 ml of reaction buffer (20 mM HEPES pH 7.4, 100 mM KAc), then 10ml of 20 mM DSP (in DMSO) was slowly added, and the suspension was incubated at room temperature for 30 min with slow shaking. The cross-linking reaction was then quenched with 10 ml of 100 mM Tris pH 7.5. Cells were then harvested and lysed as described above.

Isolation of fluorescent kinetochore particles

For examination of individual particles by total internal reflection fluorescence (TIRF) microscopy, the kinetochore material was isolated as described above, with the following modifications. Before FLAG peptide elution, beads were incubated with BH0.15 buffer (supplemented with protease inhibitors and phosphatase inhibitors) containing 30 μM SNAP-

Surface® 549 and CLIP-Surface® 647 dyes (New England Biolabs) for 25 min in the dark at room temperature. After dye-labeling, the beads were washed three times with BH0.15 (supplemented with protease inhibitors and phosphatase inhibitors) before elution. Quantification of the level of fluorescence after SDS-PAGE confirmed that the labeling reaction was specific, and that the amount of labeled protein in the eluate was maximized under these conditions (Fig. S8).

Protein and immunological techniques

Immunoblotting was performed as previously described (*8*). Commercial anti-Flag antibodies (Sigma-Aldrich) and anti-Myc antibodies (9E10, Roche) were used at 1:1,000 in PBS 0.2% tween with 1% BSA and 1% milk. Anti-Spc105 was used at 1:1,000 dilution, anti-Cse4 antibodies at 1:500 (*8*). The anti-Ndc80 (OD4, 1:10,000), anti-Mif2 (OD2, 1:6,000), and anti-Ctf19 (OD10, 1:15,000) antibodies were kind gifts from Arshad Desai (*8, 30*).

Mass spectrometry

A band of coomassie-stained gel was excised and proteins where digested using trypsin as previously described (*32*). In brief, proteins were reduced in 10 mM DTT for 30 min at 37°C, alkylated in 55 mM iodoacetamide for 20 min at room temperature in the dark, and digested overnight at 37°C with 12.5 ng μL^{-1} trypsin (Proteomics Grade, Sigma). The digestion media was then acidified to 0.1% of TFA and spun onto StageTips as described previously (*33*). Peptides were eluted in 20 µL of 80% acetonitrile in 0.1% TFA and were concentrated to 4 µL (Concentrator 5301, Eppendorf AG). The peptide sample was then diluted to 5 µL by 0.1% TFA for LC-MS/MS analysis. Analyses were performed in a Velos LTQ-Orbitrap mass spectrometer (Thermofisher Scientific) coupled on-line to a Waters Nano AQUITY UPLC (Waters), or in a Q-Exactive mass spectrometer (Thermofisher Scientific) coupled on-line to an Ultimate 3000 RSLCnano System (Thermo Fisher Scientific). Injections were performed in an analytical column with a self-assembled particle frit (*34*) and C18 material (ReproSil-Pur C18-AQ 3 µm; Dr. Maisch, GmbH) was packed into a spray emitter (75-µm ID, 8-µm opening, 300-mm length; New Objective) using an air-pressure pump (Proxeon Biosystems). Mobile phase A consisted of water and 0.1% formic acid; mobile phase B consisted of acetonitrile and 0.1% formic acid. The gradient used was 100 min. The peptides were loaded onto the column at a flow rate of 0.6 µL min^{-1} and eluted at a flow rate of 0.3 µL min^{-1} according to the gradient: 1 to 5% buffer B for 1 min, then to 32% B for 82 min, then to 35% B for 7 min and to 85% B for 5 min (Velos LTQ-Orbitrap); or at a flow rate of 0.5 µL min^{-1}, followed by elution at a flow rate of 0.2 µL min^{-1} according to the gradient: 2% to 40% buffer B for 168 min, then to 95% B for 11 min (QExactive). For the Velos LTQ-Orbitrap, FTMS spectra were recorded at 60,000 resolution and the twenty most intense peaks of the MS scan were selected in the ion trap for MS2 (normal scan, wideband activation, filling 5.0E5 ions for MS scan, 1.0E4 ions for MS2, maximum fill time 100 ms, dynamic exclusion for 60 s). For the Q-Exactive, FTMS spectra were recorded at normalized collision energy of 25, 70,000 resolution, AGC 1e6 and max filling

time of 20 ms. The 10 most intense peaks of MS scan were selected in the ion trap for MS2 (17,500 resolution, AGC 1e6, maximum fill time 60 ms, dynamic exclusion for 60s). Searches were conducted against a database containing *Saccharomyces cerevisiae* sequences (SGD – Saccharomyces Genome Database). The search parameters were: MS accuracy, 6 ppm; MS/MS accuracy, 0.6 Da; enzyme, trypsin; allowed number of missed cleavages, 2; fixed modification, carbamidometylation on cysteine; variable modification, oxidation on methionine.

Microscopy on fixed cells

Samples were analysed on a microscope (Axioplan 2; Carl Zeiss) with a 100× α Plan Fluar 1.45 NA (oil) objective lens, and images were taken using a camera (ORCA-ER; Hamamatsu Photonics) operated through Axiovision software (Carl Zeiss). Nuclei were visualized in ethanol-fixed cells by DAPI staining. 200 cells were scored at each time point. Indirect immunofluorescence was performed as previously described (*35*). Tubulin was visualized using a rat antibody at a 1:50 dilution and anti–rat FITC antibody at a 1:100 dilution. For determination of spindle morphology, 200 cells were scored at each time point. Spindle morphologies were classified as follows (also see Fig. S1D): metaphase I was defined by a single, short, bipolar spindle spanning one mass of DNA. Anaphase I was defined by an elongated spindle spanning two distinct DNA masses. Metaphase II was defined by two short, bipolar spindles, each spanning a DNA mass. Anaphase II was defined by two elongated spindles, each spanning two distinct DNA masses (four DNA masses in total).

Purification of monopolin

The *S. cerevisiae* monopolin complex was expressed and purified as previously described (*22*). Briefly, the four proteins (with protease-sensitive unstructured regions removed) were cloned into a bacterial polycistronic expression vector with an N-terminal TEV-protease cleavable His_6-tag (*36*) on Hrr25: His_6-Hrr25 2-394 (K38R)/Mam1 87-302/Csm1 1-190/Lrs4 1-102. We found that the complex was more stable when the kinase-dead K38R mutant of Hrr25 was used (*22*). Protein was expressed in *E. coli* Rosetta2 (DE3) pLysS cells (EMD Millipore) and purified using Ni-NTA (Qiagen) and ion-exchange (Hitrap SP HP, GE Life Sciences) columns. His_6-tags were cleaved with TEV protease, then the cleaved protein was passed through Ni-NTA to remove uncleaved protein and His_6-tagged TEV protease, then passed over a Superdex 200 16/600 column (GE Life Sciences). Fractions were concentrated and stored at -80°C.

Laser trap instrument

The laser trap has been described previously (*37*). Position sensor response was mapped using the piezo stage to raster-scan a stuck bead through the beam, and trap stiffness was calibrated along the two principle axes using the drag force, equipartition, and power spectrum methods. Force feedback was implemented with custom LabView software. During force measurements, bead-trap separation was sampled at 40 kHz while stage position was updated at

50 Hz to maintain the desired tension (force-clamp assay) or ramp-rate (force-ramp assay). Bead and stage position data were decimated to 200 Hz before storing to disk.

Bead functionalization and coverslip preparation for laser trap experiments

Native kinetochore particles were linked to beads as previously described (*8, 37, 38*). First, streptavidin-coated polystyrene beads (0.44 μm in diameter, Spherotech Inc., Libertyville, IL) were functionalized with biotinylated anti-His_5 antibodies (Qiagen, Valencia, CA) and stored with continuous rotation at 4 °C in BRB80 (80 mM PIPES, 1 mM $MgCl_2$, and 1 mM EGTA, pH 6.9) supplemented with 8 $mg \cdot mL^{-1}$ BSA for up to 3 months. Prior to each experiment, beads were decorated with kinetochore particles by incubating 6 pM anti-His_5 beads for 60 min at 4 °C with different amounts of the purified kinetochore material, corresponding to Dsn1-His-Flag concentrations ranging from 0.6 to 70 nM.

For laser trap experiments in which kinetochore particles were pre-incubated with recombinant monopolin in vitro (Figs. 4A-C), particles at stock concentrations ranging from 22 to 45 nM Dsn1-His-Flag were mixed with equal volumes of monopolin complex at 20, 40, 80 or 400 nM to yield molar ratios, [monopolin] • $[Dsn1]^{-1}$, between 0.44 and 8.9. Each kinetochore-monopolin mixture was pre-incubated for 30 min at 4 °C, then mixed with an equal volume of 12 pM anti-His_5 beads, and then incubated another 30 min at 4 °C prior to testing in the laser trap. For the control experiment in which kinetochore particles were first linked to beads and subsequently incubated with monopolin (Fig. 4C, open circle), meiosis I *mam1Δ* kinetochore particles at 22 nM Dsn1-His-Flag were first mixed with an equal volume of 12 pM anti-His_5 beads, incubated for 30 min at 4 °C, mixed with an equal volume of 80 nM monopolin complex, and then incubated another 30 min at 4 °C (final molar ratio, [monopolin] • $[Dsn1]^{-1}$ = 7.1). The amounts of kinetochore material for all rupture force experiments (expressed as the corresponding Dsn1-His-Flag concentration, [Dsn1], during incubation with 6 pM anti-His_5 beads), and the molar ratios ([monopolin] • $[Dsn1]^{-1}$) for all experiments involving recombinant monopolin, are given in Table S2.

Flow chambers (~10 μL volume) were made using glass slides, double-stick tape, and KOH-cleaned coverslips, and then functionalized in the following manner. First, 10 - 25 μL of 10 $mg \cdot mL^{-1}$ biotinylated BSA (Vector Laboratories, Burlingame, CA) was introduced and allowed to bind to the glass surface for 15 min at room temperature. The chamber was then washed with 100 μL of BRB80. Next, 20-100 μL of ~1 $mg \cdot mL^{-1}$ avidin DN (Vector Laboratories, Burlingame, CA) was introduced, incubated for 3 min, and washed out with 100 μL of BRB80. GMPCPP-stabilized biotinylated microtubule seeds were introduced in BRB80, and allowed to bind to the functionalized glass surface for 3 min. The chamber was then washed with 100 μL of growth buffer (BRB80 containing 1 mM GTP and 1 $mg \cdot mL^{-1}$ κ-casein). Finally, kinetochore particle-coated beads were introduced at an eightfold dilution from the incubation mix (see above) in a solution of growth buffer containing 1.5 $mg \cdot mL^{-1}$ purified bovine brain tubulin and an oxygen scavenging system (1 mM DTT, 500 $\mu g \cdot mL^{-1}$ glucose oxidase, 60 $\mu g \cdot mL^{-1}$ catalase, and 25 mM glucose). The edges of the flow chamber

were sealed to prevent evaporation. All laser trap experiments were performed in temperature-controlled rooms, maintained at 23 °C.

Binding fraction and rupture force measurements

Using the laser trap, individual free beads were placed close to the ends of growing microtubules to allow binding. Binding fraction was defined as the number of free beads that bound a microtubule divided by the total number of free beads tested. Upon binding, the attachments were preloaded with a constant force of ~4 pN. After a brief preload period, during which we verified that the beads were moving at a rate consistent with that of microtubule growth, the laser trap was programmed to ramp the force at a constant rate (0.25 pN s^{-1}) until the linkage ruptured, or until the load limit of the trap (~22 pN) was reached. ~5% of all trials ended in detachment during the preload period (i.e., before force ramping began), ~12% reached the load limit. These out-of-range events were not included in the distributions or the calculated mean rupture forces. In addition to free beads, beads found already attached (pre-bound) to microtubules were also used for the preload survival and rupture force (but not binding fraction) measurements. We found no statistically significant difference in the mean rupture force for pre-bound versus free beads that interacted with microtubules. Statistics for all data presented in this work are summarized in Table S2. All the individual rupture force values are provided in Additional Data Table S2, together with the numbers of trials that detached prematurely during the preload period or reached the load limit of the trap without rupture. *p*-values for comparison of mean rupture forces are given in Additional Data Table S3.

Imaging individual fluorescent kinetochore particles

Flow chambers were constructed as described above except that plasma-cleaned slides and coverslips were used. To provide specific binding for kinetochore particles, each chamber was first coated with a supported lipid bilayer composed of DPPC (1,2-dipalmitoyl-*sn*-glycero-3-phosphocholine; Avanti Polar Lipids, Inc.) mixed with 0.1% biotinylated PE (1,2-dipalmitoyl-*sn*-glycero-3-phosphoethanolamine-N-(cap biotinyl); Avanti). After lipid binding the chamber was washed with 35 µL of BRB80 also containing 1 mg·mL^{-1} κ-casein, and then 8 µL of 0.25 mg·mL^{-1} streptavidin (Sigma-Aldrich) in BRB80 was introduced, incubated for 5 min, and washed out with 35 µL of BRB80 plus 1 mg·mL^{-1} κ-casein. 20 µM biotinylated anti-His_5 antibodies (Qiagen, Valencia, CA) were then introduced in BRB80 plus 1 mg·mL^{-1} κ-casein, incubated for 15 min, and washed in the same way. Finally, kinetochore particles were diluted in BRB80 plus 1 mg·mL^{-1} κ-casein to a concentration corresponding to ~140 pM Dsn1, introduced into the chamber, allowed to bind 5 min, washed out, and then BRB80 plus 1 mg·mL^{-1} κ-casein with an oxygen scavenging system (see above) was flushed in. The edges of the flow chamber were sealed to prevent evaporation. Individual kinetochores immobilized on the anti-penta-his surface were viewed in a custom-built multi-color TIRF microscope with a computer-controlled 3-axis piezo specimen stage. An automated procedure was developed to rapidly record >200 images for each sample, using custom LabView software to raster the specimen stage while

maintaining image focus. All TIRF experiments were performed at room temperature. Fluorescent images of the kinetochores were filtered by a Laplacian-of-Gaussian (LOG) filter to remove the background. Individual bright spots were detected, and their brightnesses quantified by the sum of the 5 by 5 pixel area around the maxima. Custom MatLAB software was used for image processing.

Brightness distributions for fluorescent particles varied significantly from preparation to preparation, unlike mean rupture forces, which were highly reproducible. In particular, the proportion of single-color fragments lacking Nuf2 or lacking Mif2 varied between samples that were prepared, to the best of our ability, in exactly the same manner. This prep-to-prep variability made meaningful comparisons of particle brightnesses more challenging than comparisons of mean rupture forces. We therefore used two methods to control for the variability: First, to minimize the possibility for slight differences in preparation methods, we tested pairs of meiosis I and vegetative control particles that were purified and dye-labeled in tandem, on the same day. Second, to reduce the contribution of incomplete kinetochore fragments, we selected for analysis only dual-color particles carrying both Nuf2 and Mif2. Selection for both Nuf2 and Mif2 is expected to enrich for more complete kinetochore particles, since these proteins are found in the outermost (microtubule-binding) and innermost (chromatin-binding) layers of the kinetochore, respectively. A similar selection may occur in our laser trap experiments, which measure only the mechanically active, and presumably relatively complete, kinetochore particles. With these controls a clear and reproducible increase in Nuf2 content was measured for the meiosis I particles (Fig. 2E).

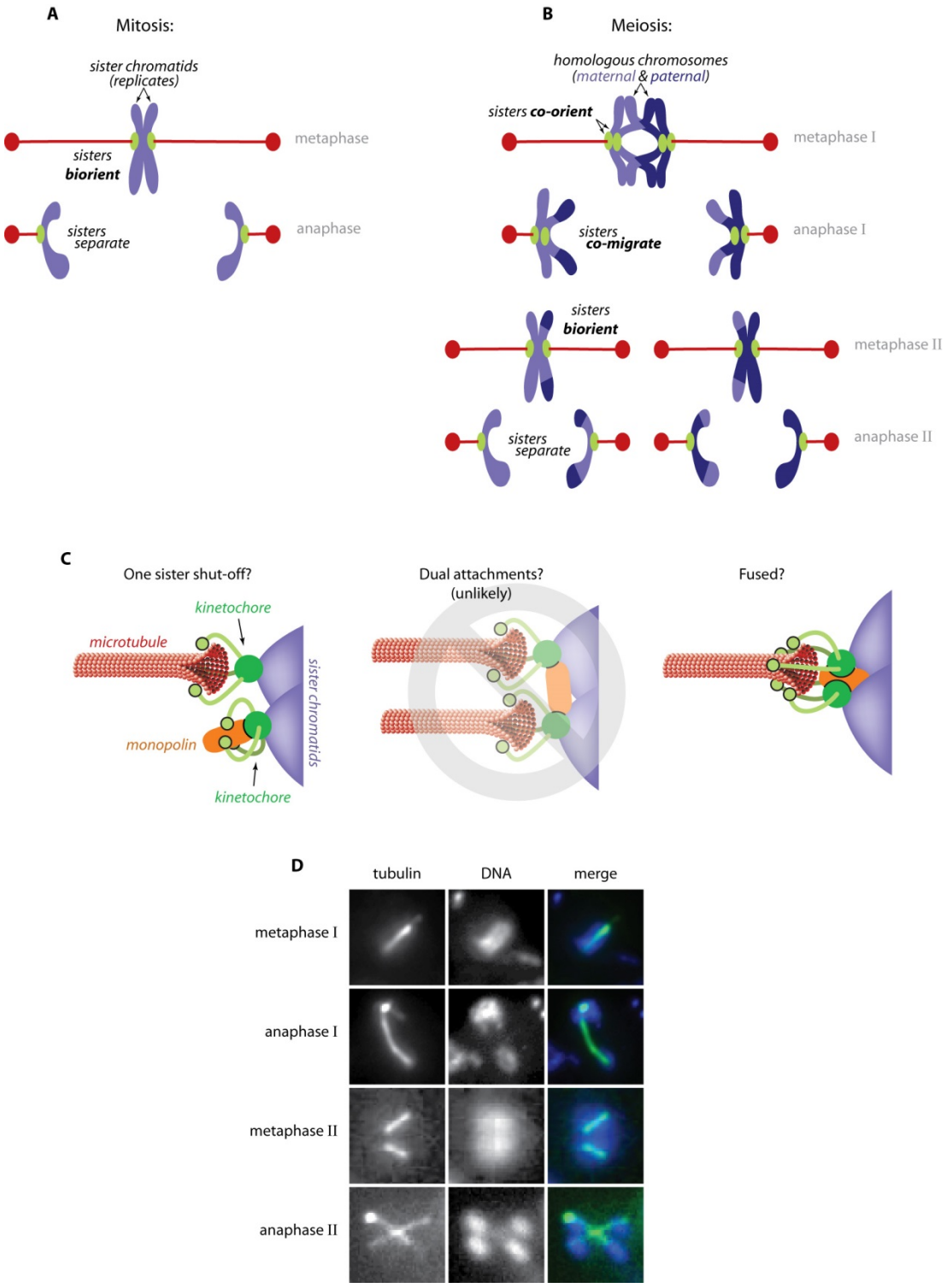

Fig. S1. Meiosis I differs fundamentally from mitosis.

(**A**) and (**B**) Replicated sister chromatids split apart during mitosis (A) and during meiosis II (B, bottom), whereas they co-migrate together during meiosis I (B, top). (**C**) Possible models for

how monopolin may promote the co-orientation of sister chromatids, and hence their co-migration, during meiosis I. First, monopolin might selectively bind and inactivate one of the two sister kinetochores (*one sister shut-off*) (*5, 6*). In this model, similar attachment strengths are predicted for meiosis I, meiosis II, and mitosis, because the active kinetochores are expected to retain similar numbers of microtubule-binding elements. Second, monopolin might hold the two sister kinetochores together so that they face in the same direction. In this case, if their microtubule-binding elements remained distinct then one might expect them to form dual attachments to a pair of microtubule tips (*dual attachments*) (*21, 23, 39, 40*). However, electron microscopy has shown that budding yeast undergoing meiosis I contain only half as many microtubules as would be required for dual attachments to every pair of sister kinetochores (*6*), so this model appears to be untenable for budding yeast. Finally, monopolin might hold sister kinetochores so closely that their microtubule binding elements cooperate together to form a single attachment site (*fused*) (*2-4*). Because a fused pair of sister kinetochores could engage a microtubule through more microtubule-binding elements, this model uniquely predicts higher strengths for isolated meiosis I kinetochore particles. We note, however, that doubling the number of microtubule-binding elements by fusing sister kinetochores will not necessarily double the rupture force: The number of elements actually bound to the microtubule may scale non-linearly if elements from the two sisters partially interfere with one another (e.g., if the microtubule tip becomes saturated before all elements are bound). Moreover, given the plasticity of kinetochore-microtubule coupling, the bound elements probably detach asynchronously, such that a complete rupture of the kinetochore-microtubule interface will not require surmounting one energy barrier equivalent to the sum of all the individual bond energies. A 'diminishing returns' scenario is likely, where rupture strength grows more slowly than the number of microtubule-binding elements. (**D**) Fluorescence images of budding yeast spindles at various stages of meiosis. Tubulin was immuno-labeled with FITC (green) and DNA was stained with DAPI (blue). In metaphase I, a bipolar spindle spans a single mass of DNA. In anaphase I, the bipolar spindle is elongated and spans two distinct DNA masses. In metaphase II, two short bipolar spindles span a DNA mass. In anaphase II, the two spindles are elongated and each one spans two distinct DNA masses (four DNA masses in total).

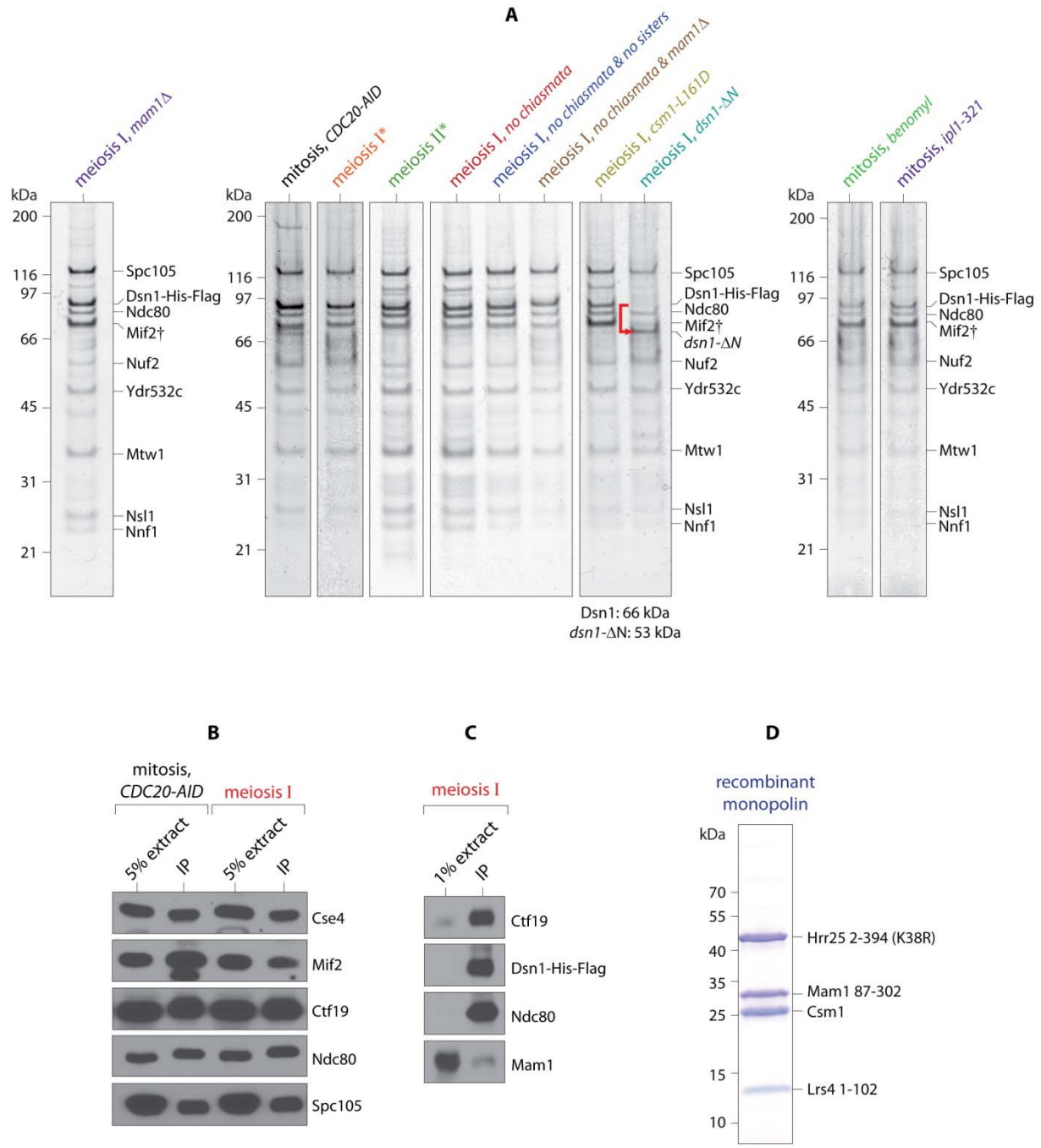

Fig. S2. The bulk composition of kinetochore material purified from mitotic and meiotic cells is similar.

(**A**) Silver-stained SDS-PAGE showing kinetochore proteins co-purified using anti-Flag antibodies. Asterisks (*) indicate preparations from cells undergoing synchronous meiosis. All other meiotic preparations are from cells arrested in metaphase I via meiosis-specific depletion of Cdc20 (*cdc20-meiotic-null*). Mitotic preparations are from cells arrested in metaphase via auxin-induced degradation of Cdc20 (*CDC20-AID*) or benomyl treatment. Mif2 (†) co-migrates

with non-specific, background proteins (*8*). (**B**) and (**C**) Immunoblots showing kinetochore components in whole cell extract and immunoprecipitate (IP, anti-Flag) from mitotic metaphase (*CDC20-AID*) and meiotic metaphase I-arrested cells. (**D**) Coommassie-stained SDS-PAGE showing the purified four-protein, kinase-dead (K38R mutant of Hrr25) monopolin complex.

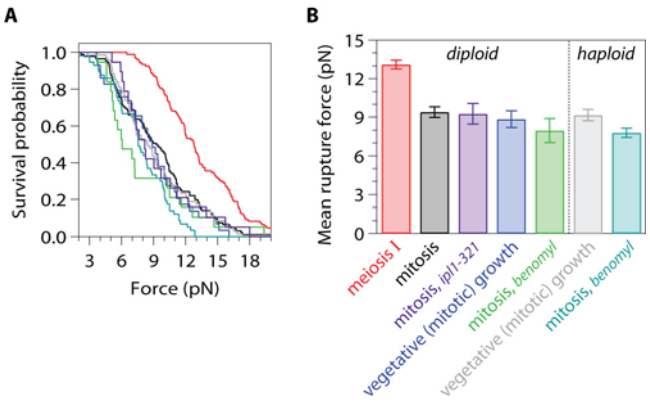

Fig. S3. The high strength of meiosis I kinetochore particles is not due to ploidy, method of arrest, or syntely.

(**A**) and (**B**) Distributions of rupture force (A) and mean rupture force values (B) for indicated kinetochore particles (color matched). Data for meiosis I and mitosis particles (red and black) are replotted from Figs. 2A and 2B for comparison. Haploid data were published previously (*8*). Error bars represent s.e.m. (N = 19-107 ruptures).

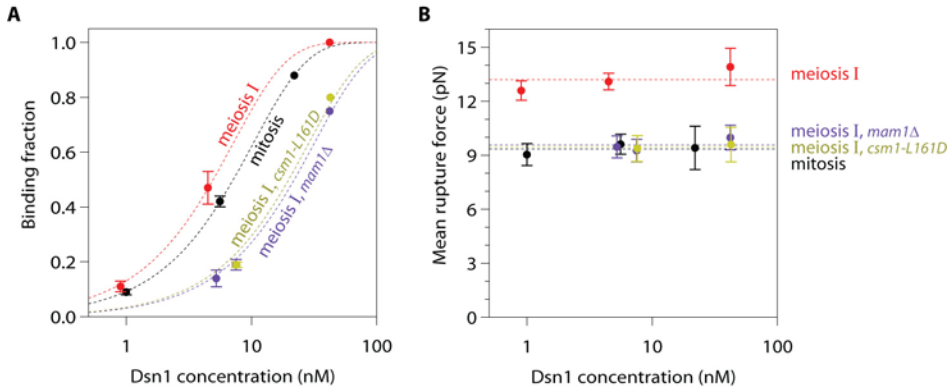

Fig. S4. Single meiotic and mitotic kinetochore particles suffice for strong attachment to dynamic microtubule tips.

(A) Fraction of beads that bound a growing microtubule tip versus concentration of kinetochore particles used to functionalize the beads. Dotted curves show Poisson fits. Error bars represent s.d. (N = 1-12 experiments). (B) Mean rupture force versus concentration of kinetochore particles used to functionalize the beads. Error bars represent s.e.m. (N = 19-56 ruptures).

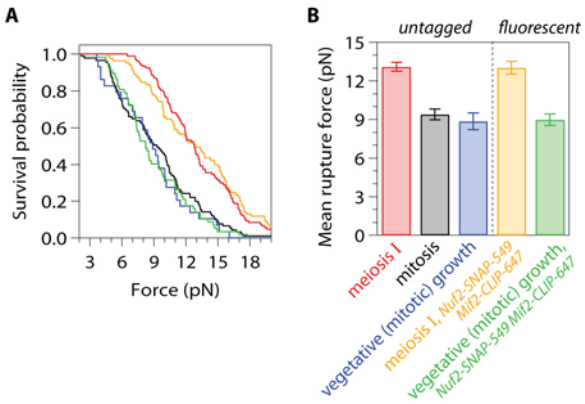

Fig. S5. Fluorescent tags on Nuf2 and Mif2 do not interfere with kinetochore particle strength.

(**A**) and (**B**) Distributions of rupture force (A) and mean rupture forces (B) for indicated kinetochore particles (color matched). Data for untagged particles from meiosis I (red), mitosis (black), and vegetative growth (blue) are replotted from Figs. 2A, 2B, S3A, and S3B, for comparison. Error bars represent s.e.m. (N = 29-107 ruptures).

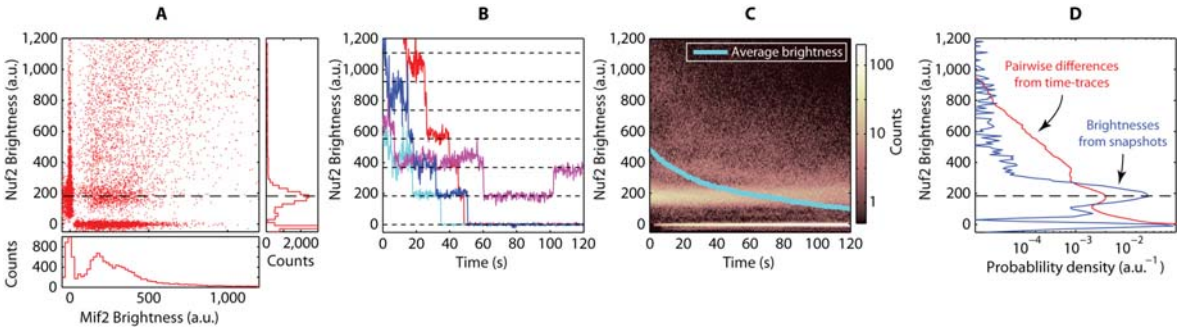

Fig. S6. Classification of fluorescent kinetochore particles and estimation of the number of Nuf2 molecules per particle.

(**A**) Bivariate plot of brightnesses determined from snapshots in two color channels (Nuf2-SNAP-549, Mif2-CLIP-647) and corresponding univariate brightness histograms (right and bottom) for N > 24,000 fluorescent meiosis I kinetochore particles bound specifically to a coverslip. The particles fall into several distinct classes, including dual-color particles with brightnesses exceeding 100 a.u. in both the Nuf2 and Mif2 channels, plus fragments lacking either Nuf2 or Mif2 (i.e., with brightnesses below 100 a.u. in either the Nuf2 or the Mif2 channel). A sub-population with just one detectable Nuf2 molecule is clearly visible (dashed line, unitary Nuf2 brightness, 180 a.u.). (**B**) Example records of Nuf2 brightness versus time showing stepwise photobleaching in increments of ~180 a.u. (**C**) Brightness versus time plotted for N = 439 particles, showing a prominent unitary population at 180 a.u. (**D**) To quantify photobleach stepsize, we computed the distribution of all pairwise brightness differences from records of brightness versus time. For the analysis shown here, only initially bright particles (i.e., those with brightness > 300 a.u. at t = 0 s) were included. The resulting pairwise difference distribution (red curve) shows a clear peak, demonstrating that these bright particles bleach in stepwise increments of 175 ± 69 a.u., equivalent to the unitary brightness from snapshots (blue curve, peak at 188 ± 32 a.u.). This correspondence indicates that the number of Nuf2 molecules in the bright particles can be estimated by dividing their brightness by the unitary brightness.

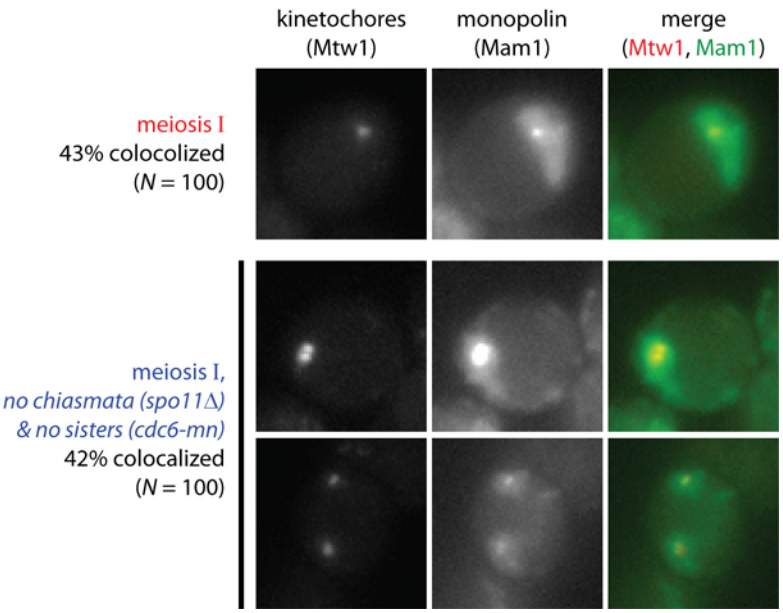

Fig. S7. Depletion of Cdc6 does not prevent recruitment of monopolin to kinetochores.

Fluorescence images of Mtw1-tomato (red) and Mam1-GFP (green) in cells arrested in metaphase I by meiosis-specific depletion of Cdc20 (*cdc20-meiotic-null*). The fraction of total imaged cells in which Mam1 colocalized with Mtw1 was similar for wild type and *spo11*Δ *cdc6-meiotic-null* strains, as shown previously (*41*).

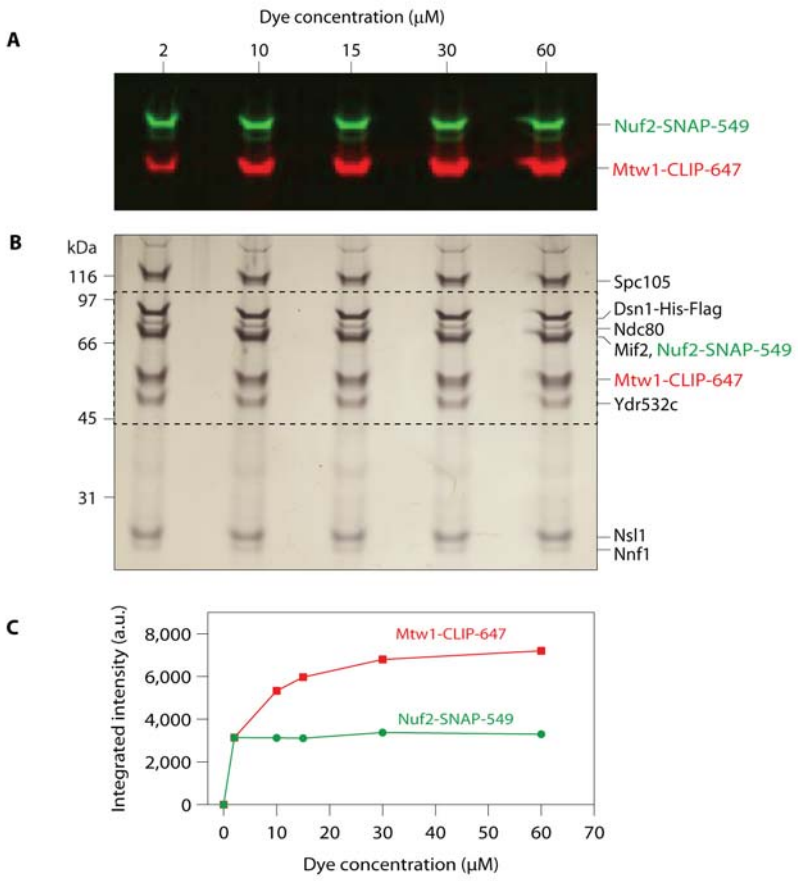

Fig. S8. Dye-labeling of SNAP- and CLIP-tagged kinetochore particles was specific and maximal.

(**A**) and (**B**) Fluorescence image (A) and corresponding silver stain (B) after incubation of immunoprecipitated kinetochore material with SNAP-Surface® 549 and CLIP-Surface® 647 at indicated concentrations, followed by separation by SDS-PAGE. The gel area shown in A corresponds to the dashed box in B. (**C**) Integrated band intensities from the image in A, plotted as a function of dye concentration.

Table S1. Mass spectrometry identifies core kinetochore subcomplexes.

Names, numbers of identified peptides, and percent coverage for core kinetochore proteins prepared from strain number AM8292 (see Table S3) are shown. All proteins identified by mass spectrometry are given in Additional Data Table S1.

		Vegetative (mitotic) growth			Meiotic metaphase I			Meiotic metaphase I with cross-linking		
Sub-complex	**Protein name**	**Total peptides**	**Unique peptides**	**% coverage**	**Total peptides**	**Unique peptides**	**% coverage**	**Total peptides**	**Unique peptides**	**% coverage**
CENP-A	**CSE4**	10	10	38.9	9	9	29.7	24	24	84.3
CENP-C	**MIF2**	47	47	70.7	37	37	61	34	34	65.8
CBF3	**CEP3**	11	11	22.9	15	15	30.9	13	13	38.2
	NDC10	-	-	-	-	-	-	38	38	51.4
	CTF13	5	5	12.6	5	5	13.4	10	10	35.1
	SKP1	1	1	10.3	2	2	19.6	-	-	-
COMA	**CTF19**	35	35	86.2	40	40	77.8	35	35	83.5
	OKP1	37	37	81.5	44	44	73.6	45	2	74.6
	MCM21	34	34	82.9	37	37	84	32	32	74.7
	AME1	26	26	77.8	31	31	82.7	29	29	75.9
SPC105 (K)	**SPC105**	106	106	78.5	128	128	85.5	79	79	70
	YDR532C	44	44	90.9	50	50	95.3	27	26	77.1
Mis12 (M)	**MTW1**	44	44	87.5	55	55	94.5	49	47	97.6
	DSN1	56	56	56.6	65	65	58	72	71	72.6
	NSL1	24	24	88.4	24	24	88.4	31	31	96.8
	NNF1	26	26	96.5	31	31	98	29	29	98
Ndc80 (N)	**NDC80**	109	109	93.3	126	126	95.5	78	77	92.2
	NUF2	56	56	78.3	66	66	86.7	37	37	86.7
	SPC24	24	24	83.6	26	26	84.5	20	20	89.7
	SPC25	19	19	81.9	25	25	91.4	19	18	78.3
Dam1	**DAM1**	16	16	51.6	24	24	60.1	12	12	47.8
	ASK1	14	14	89.4	15	15	79.5	3	3	28.4
	SPC19	13	13	83.6	13	13	83.6	3	3	49.1
	SPC34	29	29	79.7	33	33	84.7	17	17	64.7
	HSK3	5	5	58	5	5	87	1	1	30.4
	DUO1	16	16	68	22	22	89.5	10	10	80.2
	DAD1	3	3	51.1	3	3	51.1	2	2	37.2
	DAD2	2	2	15	5	5	29.3	1	1	15
	DAD3	3	3	43.6	4	4	51.1	3	3	36.2
	DAD4	3	3	47.2	4	4	55.6	1	1	34.7
CPC	**SLI15**	8	8	20.3	54	54	67.8	5	5	25.6
	BIR1	9	9	14.6	53	53	63.1	4	4	16
	IPL1	1	1	4.4	27	27	62.1	1	1	12.8
Mono-polin	**LRS4**	-	-	-	-	-	-	9	9	39.2
	CSM1	-	-	-	-	-	-	8	8	69.5
	MAM1	-	-	-	-	-	-	4	4	30.7
	HRR25	-	-	-	-	-	-	13	13	35.6
Others	**CTF3**	49	49	68.6	52	52	71.1	35	35	62.5
	CHL4	28	28	62.9	34	34	71.2	21	21	61.1
	IML3	14	14	80.8	17	17	85.7	13	13	56.3
	MCM16	6	6	43.1	9	9	58.6	14	13	99.4
	MCM22	15	15	74.5	16	16	83.7	17	17	84.1
	CNN1	9	9	38.5	8	8	26.6	7	7	34.3
	NKP1	10	10	49.2	15	15	58.8	22	21	73.1
	NKP2	6	6	50.3	8	8	72.5	8	8	67.3
	WIP2	1	1	13.5	2	2	27	-	-	-
	SLK19	9	9	17.4	74	74	77.3	11	11	31.8

Table S2. Summary of laser trap results.

Binding fractions indicate the fraction of beads that bound when held near the tip of a growing microtubule, expressed as mean ± s.d. from *N* experiments. The number of individual beads tested during each experiment ranged from 5 to 50. Rupture forces indicate mean ± s.e.m. from *N* individual rupture events. All the individual rupture force values are provided in Additional Data Table S2.

Kinetochore type	**Strain number** (ploidy)	**Metaphase arrest?** (method)	**Fraction of cells**	**[Dsn1]** (nM)	**Binding fraction**	**Mean rupture force** (pN)	**Out-of-range events***
meiosis I	AM8292 (diploid)	yes (*cdc20-mn*)	66% metaphase I	0.9	0.11 ± 0.02 (*N*=12)	12.59 ± 0.53 (*N*=31)	*a*=4; *b*=7
				4.5	0.47 ± 0.06 (*N*=3)	13.09 ± 0.47 (*N*=56)	*a*=4; *b*=13
				42.0	1.00 ± 0.00 (*N*=2)	13.91 ± 1.03 (*N*=20)	*a*=3; *b*=30
mitosis	AM10622 (diploid)	yes (*CDC20-AID*)	66% metaphase	1.0	0.09 ± 0.01 (*N*=3)	9.04± 0.61 (*N*=28)	*a*=2; *b*=5
				5.6	0.42 ± 0.02 (*N*=2)	9.61± 0.56 (*N*=44)	*a*=2; *b*=10
				22.0	0.88 (*N*=1)	9.41± 1.20 (*N*=19)	*a*=1; *b*=2
*+recombinant monopolin **in vitro**,* [monopolin]•[Dsn]$^{-1}$ = 3.6				5.6	0.50 ± 0.00 (*N*=2)	13.08 ± 0.63 (*N*=24)	*a*=0; *b*=4
meiosis I*, *synchronous* (Ndt80 block-release)	AM11158 (diploid)	no	57% metaphase I	4.5	0.48 ± 0.03 (*N*=3)	13.07 ± 0.64 (*N*=15)	*a*=22; *b*=1
meiosis II*, *synchronous* (Ndt80 block-release)	AM11158 (diploid)	no	85% binucleated	5.0	0.50 ± 0.00 (*N*=2)	9.30 ± 0.73 (*N*=30)	*a*=1; *b*=9
meiosis I, *no chiasmata* (*spo11Δ*)	AM11647 (diploid)	- (*cdc20-mn*) †	65% meiosis I	6.0	0.50 (*N*=1)	13.23 ± 0.73 (*N*=27)	*a*=2; *b*=16
meiosis I, *no sisters* (*cdc6-mn*)	AM11689 (diploid)	yes (*cdc20-mn*)	63% meiosis I	6.0	0.42 ± 0.02 (*N*=2)	9.27 ± 0.79 (*N*=30)	*a*=4; *b*=2
meiosis I, *no chiasmata* (*spo11Δ*) *& no sisters* (*cdc6-mn*)	AM11710 (diploid)	- (*cdc20-mn*) †	61% meiosis I	6.0	0.47 ± 0.04 (*N*=2)	9.44 ± 0.74 (*N*=35)	*a*=4; *b*=4
meiosis I, *no monopolin* (*mam1Δ*)	AM10455 (diploid)	yes (*cdc20-mn*)	67% metaphase I	5.25	0.14 ± 0.03 (*N*=3)	9.47 ± 0.61 (*N*=43)	*a*=6; *b*=5
				7.5	0.19 ± 0.02 (*N*=3)	9.26 ± 0.63 (*N*=46)	*a*=2; *b*=6
				42.0	0.75 (*N*=1)	9.99 ± 0.68 (*N*=29)	*a*=0; *b*=7
*+recombinant monopolin **in vitro**,* [monopolin]•[Dsn]$^{-1}$ = 0.44				11.3	0.25 (*N*=1)	10.19 ± 0.55 (*N*=64)	*a*=1; *b*=6
*+recombinant monopolin **in vitro**,* [monopolin]•[Dsn]$^{-1}$ = 0.89				11.3	0.24 ± 0.02 (*N*=2)	11.29 ± 0.88 (*N*=30)	*a*=2; *b*=5
*+recombinant monopolin **in vitro**,* [monopolin]•[Dsn]$^{-1}$ = 1.8				11.3	0.23 ± 0.03 (*N*=3)	13.21 ± 0.48 (*N*=57)	*a*=3; *b*=12
*+recombinant monopolin **in vitro**,* [monopolin]•[Dsn]$^{-1}$ = 8.9				11.3	-	13.14 ± 0.80 (*N*=28)	*a*=0; *b*=5
+recomb. monopolin after bead linkage, [monopolin]•[Dsn]$^{-1}$ = 7.1				11.3	0.25 ± 0.00 (*N*=2)	9.31 ± 0.80 (*N*=29)	*a*=0; *b*=1
meiosis I, *monopolin point mutant* (*csm1-L161D*)	AM12390 (diploid)	yes (*cdc20-mn*)	74% metaphase I	7.6	0.19 ± 0.01 (*N*=2)	9.37 ± 0.73 (*N*=33)	*a*=3; *b*=5
				42.6	0.80 (*N*=1)	9.59 ± 0.96 (*N*=24)	*a*=0; *b*=9
*+recombinant monopolin **in vitro**,* [monopolin]•[Dsn]$^{-1}$ = 1.8				11.3	-	13.26 ± 0.89 (*N*=24)	*a*=0; *b*=0

Kinetochore type	**Strain number** (ploidy)	**Metaphase arrest?** (method)	**Fraction of cells**	**[Dsn1]** (nM)	**Binding fraction**	**Mean rupture force** (pN)	**Out-of-range events***
meiosis I, *no chiasmata* (*spo11Δ*) *& no monopolin* (*mam1Δ*)	AM12539 (diploid)	yes (*cdc20-mn*)	58% metaphase I	7.5	0.23 ± 0.04 (*N*=2)	9.11 ± 0.85 (*N*=31)	*a*=2; *b*=3
meiosis I, *truncated Dsn1* (*dsn1-ΔN*)	AM12285 (diploid)	yes (*cdc20-mn*)	71% metaphase I	15.0	0.83 (*N*=1)	9.37 ± 1.04 (*N*=21)	*a*=0; *b*=2
*+recombinant monopolin **in vitro**,* [monopolin]•[Dsn]$^{-1}$ = 2.1				9.5	0.75 (*N*=1)	9.28 ± 1.21 (*N*=17)	*a*=0; *b*=1
mitosis, *+ectopic monopolin induction **in vivo***	AM12111 (diploid)	yes (*CDC20-AID*)	84% metaphase	6.0	0.45 ± 0.07 (*N*=2)	11.16± 0.45 (*N*=65)	*a*=0; *b*=1
mitosis, *with mono-orientation* (*ipl-321*)	AM11789 (diploid)	yes (*CDC20-AID*)	76% metaphase	6.0	0.23 ± 0.04 (*N*=2)	9.26 ± 0.82 (*N*=19)	*a*=1; *b*=1
vegetative growth	AM8292 (diploid)	no	n/a	3.75	0.23 ± 0.05 (*N*=2)	9.04 ± 0.64 (*N*=28)	*a*=3; *b*=1
mitosis, *benomyl*	AM8292 (diploid)	yes (benomyl)	>80% mitotic	7.5	0.50 (*N*=1)	7.98 ± 0.95 (*N*=19)	*a*=0; *b*=2
vegetative growth ‡	SBY8253 (haploid)	no	n/a	6.0	0.52 ± 0.04 (*N*=7)	9.18 ± 0.45 (*N*=69)	*a*=10; *b*=12
mitosis, *benomyl* ‡	SBY8253 (haploid)	yes (benomyl)	-	6.0	0.45 ± 0.11 (*N*=4)	7.78 ± 0.36 (*N*=57)	*a*=8; *b*=7
vegetative growth, *truncated Dsn1* (*dsn1-ΔN*)	AM12285 (diploid)	no	n/a	6.0	0.50 (*N*=1)	9.19 ± 0.69 (*N*=18)	*a*=0; *b*=4
*+recombinant monopolin **in vitro**,* [monopolin]•[Dsn]$^{-1}$ = 2.2				9.0	0.75 (*N*=1)	9.46 ± 0.86 (*N*=17)	*a*=0; *b*=2
fluorescent prep pair #1, meiosis I	AM13794 (diploid)	yes (*cdc20-mn*)	70% metaphase I	7.5	-	13.65 ± 1.16 (*N*=22)	*a*=0; *b*=4
vegetative growth		no	n/a	6.0	-	9.09 ± 0.76 (*N*=17)	*a*=0; *b*=2
fluorescent prep pair #2, meiosis I	AM13794 (diploid)	yes (*cdc20-mn*)	57% metaphase I	7.5	0.13 (*N*=1)	12.92 ± 1.32 (*N*=11)	*a*=0; *b*=1
vegetative growth		no	n/a	7.5	0.40 (*N*=1)	8.73 ± 0.76 (*N*=16)	*a*=0; *b*=0
fluorescent prep pair #3, meiosis I	AM13794 (diploid)	yes (*cdc20-mn*)	61% metaphase I	6.0	0.20 (*N*=1)	12.90 ± 1.14 (*N*=17)	*a*=1; *b*=2
vegetative growth		no	n/a	6.0	0.17 (*N*=1)	8.53 ± 2.46 (*N*=4)	*a*=1; *b*=0
fluorescent prep pair #4, meiosis I	AM13794 (diploid)	yes (*cdc20-mn*)	56% metaphase I	6.0	0.50 (*N*=1)	12.74 ± 0.70 (*N*=35)	*a*=5; *b*=13
vegetative growth		no	n/a	6.0	0.50 (*N*=1)	9.22 ± 0.83 (*N*=20)	*a*=0; *b*=0

*The number of trials that ended in premature detachment during the preload period before force ramping began, and the number that reached the load limit of the trap before rupture occurred, are represented by *a* and *b*, respectively. These out-of-range events were not included in the calculations of mean rupture force.

†*cdc20-mn spo11Δ* cells have been reported to arrest in metaphase II (*42*); but at the time we harvested these cells for kinetochore purification, the majority (> 60%, as indicated above) appeared to have meiosis I spindles.

‡Data from ref [(*8*)].

Table S3. Yeast strains used in this study.

All strains are isogenic with the SK1 background, except strain SBY8253, which is isogenic with W303.

Strain number	Kinetochore type(s)	Relevant genotype	Used in figure
AM8292	meiosis I, mitosis, *benomyl*, and vegetative growth	*MATa/MATalpha* *DSN1-6HIS-3FLAG::URA3/DSN1-6HIS-3FLAG::URA3* *cdc20::pCLB2-3HA-CDC20::KANMX6/cdc20::pCLB2-3HA-CDC20::KANMX6*	1A, 1C, 1D, 2A, 2B, 3A, 3B, 4A, 4B, S2A, S2B, S3A, S3B, S4A, S4B, S5A, S5B
AM10455	meiosis I, *no monopolin* (*mam1Δ*)	*MATa/MATalpha* *cdc20::pCLB2-CDC20::KANMX6/cdc20::pCLB2-CDC20::KANMX6* *mam1Δ::KANMX6/mam1Δ::KANMX6* *DSN1-6HIS-3FLAG:URA3/DSN1-6HIS-3FLAG:URA3*	3A, 3B, 4A, 4B, 4C, S2A, S4A, S4B
AM10622	mitosis	*MATa/MATalpha* *CDC20-AID::KANMX6/CDC20-AID::KANMX6* *ura3::pADH1-OsTIR1-9MYC::URA3/ura3::pADH1-OsTIR1-9MYC::URA3* *DSN1-6HIS-3FLAG::URA3/DSN1-6HIS-3FLAG::URA3*	1D, 2A, 2B, 3A, 3B, 4A, 4B, S2A, S2B, S3A, S3B, S4A, S4B, S5A, S5B
AM11158	meiosis I* and meiosis II*, *synchronous* (Ndt80 block-release)	*MATa/MATalpha* *DSN1-6HIS-3FLAG::URA3/DSN1-6HIS-3FLAG::URA3* *GAL-NDT80::TRP1/GAL-NDT80::TRP1* *ura3::pGPD1-GAL4(848).ER::URA3/ura3::pGPD1-GAL4(848).ER::URA3*	2A, 2B, S2A
AM11647	meiosis I, *no chiasmata* (*spo11Δ*)	*MATa/MATalpha* *cdc20::pCLB2-CDC20::KANMX6/cdc20::pCLB2-CDC20::KANMX6* *DSN1-6HIS-3FLAG:URA3/DSN1-6HIS-3FLAG:URA3* *spo11::URA3/spo11::URA3* *NDC10-6HA:HIS3MX6/+* *MAM1-9MYC:TRP1/+*	2A, 2B, 3A, 3B, S2A
AM11689	meiosis I, *no sisters* (*cdc6-mn*)	*MATa/MATalpha* *cdc20::pCLB2-CDC20::KANMX6/cdc20::pCLB2-CDC20::KANMX6* *cdc6::KANMX6::pSCC1-3HA-CDC6/cdc6::KANMX6::pSCC1-3HA-CDC6* *DSN1-6HIS-3FLAG:URA3/DSN1-6HIS-3FLAG:URA3*	2A, 2B
AM11710	meiosis I, *no chiasmata* (*spo11Δ*) *& no sisters* (*cdc6-mn*)	*MATa/MATalpha* *spo11::URA3/spo11::URA3* *cdc20::pCLB2-CDC20::KANMX6/cdc20::pCLB2-CDC20::KANMX6* *cdc6::KANMX6::pSCC1-3HA-CDC6/cdc6::KANMX6::pSCC1-3HA-CDC6* *DSN1-6HIS-3FLAG:URA3/DSN1-6HIS-3FLAG:URA3*	2A, 2B, S2A
AM11789	mitosis, *with mono-orientation* (*ipl-321*)	*MATa/MATalpha* *CDC20-AID::KANMX6/CDC20-AID::KanMX6* *ura3::pADH1-OsTIR1-9MYC::URA3/ura3::pADH1-OsTIR1-9MYC::URA3* *DSN1-6HIS-3FLAG::URA3/DSN1-6HIS-3FLAG::URA3* *ipl1-321:KANMX6/ipl1-321:KANMX6* *CENV::tetOx224::HIS3/+* *promURA3::TetR::GFP::LEU2/+*	S2A, S3A, S3B
AM12111	mitosis, *+ectopic monopolin induction **in vivo***	*MATa/MATalpha* *GAL3+/GAL3+* *CDC20-AID::KANMX6/CDC20-AID::KANMX6* *ura3::pADH1-OsTIR1-9MYC::URA3/ura3::pGAL1-3MYC-CDC5::URA3* *DSN1-6HIS-3FLAG::URA3/DSN1-6HIS-3FLAG::URA3* *MAM1::pGAL1-3HA-MAM1::TRP1/MAM1::pGAL1-3HA-MAM1::TRP1* *promURA3::TetR::GFP::LEU2/+* *CENV::tetOx224::HIS3/+*	3A, 3B
AM12285	meiosis I, *truncated Dsn1* (*dsn1-ΔN*)	*MATa/MATalpha* *cdc20::pCLB2-3HA-CDC20::KANMX6/cdc20::pCLB2-3HA-CDC20::KANMX6* *dsn1::Δ110DSN1-6HIS-3FLAG::URA3/dsn1::Δ110DSN1-6HIS-3FLAG::URA3* *promURA3::TetR::GFP::LEU2/+* *CENV::tetOx224::HIS3/+*	3A, 3B, 4A, 4B, S2A
AM12390	meiosis I, *monopolin point mutant* (*csm1-L161D*)	*MATa/MATalpha* *DSN1-6HIS-3FLAG::URA3/DSN1-6HIS-3FLAG::URA3* *cdc20::pCLB2-3HA-CDC20::KANMX6/cdc20::pCLB2-3HA-CDC20::KANMX6* *leu::pURA3-TetR-GFP::LEU2/+* *CENV::tetOx224::HIS3/+* *csm1(L161D)::KANMX6/csm1(L161D)::KANMX6*	3A, 3B, 4A, 4B, S2A, S4A, S4B

Strain number	Kinetochore type(s)	Relevant genotype	Used in figure
AM12539	meiosis I, *no chiasmata* (*spo11Δ*) *& no monopolin* (*mam1Δ*)	*MATa/MATalpha* *cdc20::pCLB2-3HA-CDC20::KANMX6/cdc20::pCLB2-3HA-CDC20::KANMX6* *DSN1-6HIS-3FLAG::URA3/DSN1-6HIS-3FLAG::URA3* *mam1Δ::KANMX6/mam1Δ::KANMX6* *spo11Δ::NATMX/spo11Δ::NATMX*	3A, 3B, S2A
AM13794	fluorescent kinetochores, meiosis I and vegetative growth (Nuf2-SNAP, Mif2-CLIP)	*MATa/MATalpha* *cdc20::pCLB2-CDC20::KANMX6/cdc20::pCLB2-CDC20::KANMX6* *DSN1-6HIS-3FLAG:URA3/DSN1-6HIS-3FLAG:URA3* *NUF2-fSNAP::HPH/NUF2-fSNAP::HPH* *MIF2-fCLIP:NATMX6/MIF2-fCLIP:NATMX6* *MAM1-9MYC:TRP1/+* *NDC10-6HA:HIS3MX6/+*	1B, 2C, 2D, 2E, 4D, S5A, S5B, S6A, S6B, S6C, S6D
AM13558	meiosis I (Mtw1-tomato & Mam1-GFP)	*MATa/MATalpha* *cdc20::pCLB2-CDC20::KANMX6/cdc20::pCLB2-CDC20::KANMX6* *MAM1-yeGFP::KITRP1/MAM1-yeGFP::KITRP1* *MTW1-tdTomato::NAT/MTW1-tdTomato::NAT*	S7
AM13565	meiosis I, *no chiasmata* (*spo11Δ*) *& no sisters* (*cdc6-mn*), (Mtw1-tomato & Mam1-GFP)	*MATa/MATalpha* *cdc20::pCLB2-CDC20::KANMX6/cdc20::pCLB2-CDC20::KANMX6* *spo11::URA3/ spo11::URA3* *cdc6::KANMX6::pSCC1-3HA-CDC6/cdc6::KANMX6::pSCC1-3HA-CDC6* *MAM1-yeGFP::KITRP1/MAM1-yeGFP::KITRP1* *MTW1-tdTomato::NAT/MTW1-tdTomato::NAT*	S7
AM14361	meiosis I (Mam1-9myc, for Western)	*MATa/MATalpha* *cdc20::pCLB2-CDC20::KANMX6/cdc20::pCLB2-CDC20::KANMX6* *DSN1-6HIS-3FLAG:URA3/DSN1-6HIS-3FLAG:URA3* *NDC10-6HA:HIS3MX6/NDC10-6HA:HIS3MX6* *MAM1-9MYC:TRP1/MAM1-9MYC:TRP1*	S2C
SBY8253	mitosis, *benomyl*, and vegetative growth (haploid)	*MATa* *ura3-1 leu2,3-112 his3-11 trp1-1 ade2-1 can1-100 LYS2 bar1Δ* *DSN1-6HIS-3FLAG::URA3*	S3A, S3B

Movie S1. Meiotic kinetochore particles bind microtubules and track with disassembling tips.

Dynamic microtubules were polymerized from Alexa-488-labeled tubulin in the presence of fluorescent kinetochore particles, purified from strain AM13794 and dye-labeled as described in Materials and Methods. Depolymerization was triggered by removing the free tubulin via buffer exchange, causing disassembly-driven movement of microtubule-bound kinetochore particles.

Additional Data Table S1. All proteins identified by mass spectrometry.

Names, numbers of identified peptides, and percent coverage for all proteins identified by mass spectrometry are provided in the accompanying spreadsheet (Excel file link).

Additional Data Table S2. All individual rupture force values.

The individual rupture force values for all rupture events are listed in the accompanying spreadsheet (Excel file link). Mean rupture forces and standard errors (Figs. 2-4, S3-S5, and Table S2) were computed arithmetically from these individual values.

Additional Data Table S3. Statistical comparison of rupture strengths for all measured kinetochore types.

p-values for comparison of mean rupture forces for different kinetochore types at comparable Dsn1 concentrations (see Table S2) are summarized in the accompanying spreadsheet (Excel file link). We employed the criterion that $p > 0.1$ indicates lack of statistical significance (red) while $p < 0.05$ indicates a statistically significant difference (green) between the compared means.

References and Notes

1. K. D. Corbett *et al.*, The monopolin complex crosslinks kinetochore components to regulate chromosome-microtubule attachments. *Cell* **142**, 556 (2010).
2. X. Li, R. K. Dawe, Fused sister kinetochores initiate the reductional division in meiosis I. *Nat Cell Biol* **11**, 1103 (2009).
3. L. S. Goldstein, Kinetochore structure and its role in chromosome orientation during the first meiotic division in male D. melanogaster. *Cell* **25**, 591 (1981).
4. L. V. Paliulis, R. B. Nicklas, The reduction of chromosome number in meiosis is determined by properties built into the chromosomes. *J Cell Biol* **150**, 1223 (2000).
5. F. Monje-Casas, V. R. Prabhu, B. H. Lee, M. Boselli, A. Amon, Kinetochore orientation during meiosis is controlled by Aurora B and the monopolin complex. *Cell* **128**, 477 (2007).
6. M. Winey, G. P. Morgan, P. D. Straight, T. H. Giddings, Jr., D. N. Mastronarde, Three-dimensional ultrastructure of Saccharomyces cerevisiae meiotic spindles. *Mol Biol Cell* **16**, 1178 (2005).
7. B. H. Lee, A. Amon, Role of Polo-like kinase CDC5 in programming meiosis I chromosome segregation. *Science* **300**, 482 (2003).
8. B. Akiyoshi *et al.*, Tension directly stabilizes reconstituted kinetochore-microtubule attachments. *Nature* **468**, 576 (2010).
9. Materials and methods are available as supplementary materials online.
10. T. M. Carlile, A. Amon, Meiosis I is established through division-specific translational control of a cyclin. *Cell* **133**, 280 (2008).
11. K. R. Benjamin, C. Zhang, K. M. Shokat, I. Herskowitz, Control of landmark events in meiosis by the CDK Cdc28 and the meiosis-specific kinase Ime2. *Genes Dev* **17**, 1524 (2003).
12. A. P. Joglekar, D. C. Bouck, J. N. Molk, K. S. Bloom, E. D. Salmon, Molecular architecture of a kinetochore-microtubule attachment site. *Nat Cell Biol* **8**, 581 (2006).
13. J. Lawrimore, K. S. Bloom, E. D. Salmon, Point centromeres contain more than a single centromere-specific Cse4 (CENP-A) nucleosome. *J Cell Biol* **195**, 573 (2011).
14. A. Hochwagen, W. H. Tham, G. A. Brar, A. Amon, The FK506 binding protein Fpr3 counteracts protein phosphatase 1 to maintain meiotic recombination checkpoint activity. *Cell* **122**, 861 (2005).
15. J. H. Cocker, S. Piatti, C. Santocanale, K. Nasmyth, J. F. Diffley, An essential role for the Cdc6 protein in forming the pre-replicative complexes of budding yeast. *Nature* **379**, 180 (1996).

16. T. Goldfarb, M. Lichten, Frequent and efficient use of the sister chromatid for DNA double-strand break repair during budding yeast meiosis. *PLoS biology* **8**, e1000520 (2010).
17. S. Keeney, C. N. Giroux, N. Kleckner, Meiosis-specific DNA double-strand breaks are catalyzed by Spo11, a member of a widely conserved protein family. *Cell* **88**, 375 (1997).
18. M. A. Shonn, R. McCarroll, A. W. Murray, Requirement of the spindle checkpoint for proper chromosome segregation in budding yeast meiosis. *Science* **289**, 300 (2000).
19. M. Petronczki *et al.*, Monopolar attachment of sister kinetochores at meiosis I requires casein kinase 1. *Cell* **126**, 1049 (2006).
20. K. P. Rabitsch *et al.*, Kinetochore recruitment of two nucleolar proteins is required for homolog segregation in meiosis I. *Dev Cell* **4**, 535 (2003).
21. A. Toth *et al.*, Functional genomics identifies monopolin: a kinetochore protein required for segregation of homologs during meiosis i. *Cell* **103**, 1155 (2000).
22. K. D. Corbett, S. C. Harrison, Molecular architecture of the yeast monopolin complex. *Cell reports* **1**, 583 (2012).
23. S. Sarkar *et al.*, Monopolin Subunit Csm1 Associates with MIND Complex to Establish Monopolar Attachment of Sister Kinetochores at Meiosis I. *PLoS Genet* **9**, e1003610 (2013).
24. K. T. Jones, S. I. Lane, Molecular causes of aneuploidy in mammalian eggs. *Development* **140**, 3719 (2013).
25. M. Knop *et al.*, Epitope tagging of yeast genes using a PCR-based strategy: more tags and improved practical routines. *Yeast* **15**, 963 (1999).
26. M. S. Longtine *et al.*, Additional modules for versatile and economical PCR-based gene deletion and modification in Saccharomyces cerevisiae. *Yeast* **14**, 953 (1998).
27. J. F. Charles *et al.*, The Polo-related kinase Cdc5 activates and is destroyed by the mitotic cyclin destruction machinery in S. cerevisiae. *Current biology : CB* **8**, 497 (1998).
28. S. Biggins *et al.*, The conserved protein kinase Ipl1 regulates microtubule binding to kinetochores in budding yeast. *Genes Dev* **13**, 532 (1999).
29. I. Shcherbakova *et al.*, Alternative spliceosome assembly pathways revealed by single-molecule fluorescence microscopy. *Cell reports* **5**, 151 (2013).
30. B. Akiyoshi, C. R. Nelson, J. A. Ranish, S. Biggins, Quantitative proteomic analysis of purified yeast kinetochores identifies a PP1 regulatory subunit. *Genes Dev* **23**, 2887 (2009).
31. K. Nishimura, T. Fukagawa, H. Takisawa, T. Kakimoto, M. Kanemaki, An auxin-based degron system for the rapid depletion of proteins in nonplant cells. *Nat Meth* **6**, 917 (2009).

32. A. Shevchenko, M. Wilm, O. Vorm, M. Mann, Mass spectrometric sequencing of proteins silver-stained polyacrylamide gels. *Anal Chem* **68**, 850 (1996).
33. J. Rappsilber, Y. Ishihama, M. Mann, Stop and go extraction tips for matrix-assisted laser desorption/ionization, nanoelectrospray, and LC/MS sample pretreatment in proteomics. *Anal Chem* **75**, 663 (2003).
34. Y. Ishihama, J. Rappsilber, J. S. Andersen, M. Mann, Microcolumns with self-assembled particle frits for proteomics. *Journal of chromatography. A* **979**, 233 (2002).
35. R. Visintin, E. S. Hwang, A. Amon, Cfi1 prevents premature exit from mitosis by anchoring Cdc14 phosphatase in the nucleolus. *Nature* **398**, 818 (1999).
36. R. B. Kapust *et al.*, Tobacco etch virus protease: mechanism of autolysis and rational design of stable mutants with wild-type catalytic proficiency. *Protein engineering* **14**, 993 (2001).
37. A. D. Franck, A. F. Powers, D. R. Gestaut, T. N. Davis, C. L. Asbury, Direct physical study of kinetochore-microtubule interactions by reconstitution and interrogation with an optical force clamp. *Methods* **51**, 242 (2010).
38. K. K. Sarangapani, B. Akiyoshi, N. M. Duggan, S. Biggins, C. L. Asbury, Phosphoregulation promotes release of kinetochores from dynamic microtubules via multiple mechanisms. *Proc Natl Acad Sci U S A* **110**, 7282 (2013).
39. A. L. Marston, A. Amon, Meiosis: cell-cycle controls shuffle and deal. *Nat Rev Mol Cell Biol* **5**, 983 (2004).
40. M. Petronczki, M. F. Siomos, K. Nasmyth, Un menage a quatre: the molecular biology of chromosome segregation in meiosis. *Cell* **112**, 423 (2003).
41. J. Matos *et al.*, Dbf4-dependent CDC7 kinase links DNA replication to the segregation of homologous chromosomes in meiosis I. *Cell* **135**, 662 (2008).
42. M. A. Attner, M. P. Miller, L. S. Ee, S. K. Elkin, A. Amon, Polo kinase Cdc5 is a central regulator of meiosis I. *Proc Natl Acad Sci U S A* **110**, 14278 (2013).